ELECTROCHEMICAL METHOD FOR CHARACTERIZATION AND RANKING OF CORROSION INHIBITORS

A Thesis
Submitted to the Graduate Faculty
of the
North Dakota State University
of Agriculture and Applied Science

By

Brett Matthew Kelly

In Partial Fulfillment of the Requirements
for the Degree of
MASTER OF SCIENCE

Major Department:
Coatings and Polymeric Materials

November 2017

Fargo, North Dakota

North Dakota State University
Graduate School

Title

ELECTROCHEMICAL METHOD FOR CHARACTERIZATION AND RANKING OF CORROSION INHIBITORS

By

Brett Matthew Kelly

The Supervisory Committee certifies that this ***disquisition*** complies with North Dakota State University's regulations and meets the accepted standards for the degree of

MASTER OF SCIENCE

SUPERVISORY COMMITTEE:

Dante Battocchi
Chair

Shannon David

Mohiuddin Quadir

Andriy Voronov

Approved:

November 30, 2017 — Date

Dean Webster — Department Chair

ABSTRACT

One of the most cost-effective methods in mitigating corrosion effects is through the use of corrosion inhibitors. This work studied the performance of eight organic inhibitors on mild steel substrate through electrochemical characterization techniques, with the primary goal of incorporating a screening process to sift through the large selection of potential inhibitors without having to fully characterize them.

The test methodology developed was successful at screening the potential corrosion inhibitors through linear polarization resistance (LPR) testing in NaCl electrolyte, narrowing the collection of inhibitors to the three most-promising chemicals, adrenalone, 3,4-dihydroxyphenylacetic acid and dopamine. The screened inhibitors proved effective in HCl electrolyte, reducing the corrosion rates of mild steel by over 85%. X-ray photoelectron spectroscopy (XPS) and quartz crystal microbalance (QCM) testing were used to confirm surface adsorption of the molecules to the substrate, indicating the formation of a protective barrier film as the means of corrosion protection.

ACKNOWLEDGEMENTS

I would like to take the opportunity to express my gratitude to Dr. Dante Battocchi for all of his help, advice and continued support, as both an advisor and friend, during my entire graduate process. I would also like to acknowledge Dr. Shannon David, Dr. Mohiuddin Quadir, and Dr. Andriy Voronov for taking the time to serve on my supervisory committee and providing the guidance necessary to improve my work. The enthusiasm with which each of you pursue your own research endeavors is refreshing and such a motivation to us graduate students.

Also, a huge thanks to Dr. Vinod Upadhyay and Dr. Xiaoning Qi for their immense help and advice with the electrochemical techniques, and to Jim Bahr for the help with XPS characterization. Additionally, I am grateful to all the faculty, staff and students of the Department of Coatings and Polymeric Materials at North Dakota State University for making my experience here an enjoyable one.

Finally, I must express my greatest gratitude to the best friend I never deserved. Ann, thank you for being the one I look forward to seeing each and every day – I don't know where I would be without you.

DEDICATION

This work is dedicated to my mother and father;

for their eternal support and encouragement, and for allowing me to freely discover

the man I wanted to become.

TABLE OF CONTENTS

LIST OF TABLES

LIST OF FIGURES

CHAPTER 1. INTRODUCTION TO CARBON STEEL CORROSION, PREVENTION STRATEGIES, AND A DISCUSSION ON INHIBITORS

1.1. Introduction to Corrosion

Corrosion is a natural chemical process that effectively degrades the surfaces of metals when they come in contact with corrosive environments, such as salt-laden sea water, chemical treatment streams in industrial settings, or even water vapor in the atmosphere. Corrosion is a process that is almost exclusively never desired, as it often poses a safety concern and has immense economic implications. Corrosion affects the infrastructure, manufacturing and production, utilities, government and transportation sectors. It is difficult to account for the entire economic cost of corrosion, as the indirect costs of lost productivity, plant downtime, or impacts of events such as power outages are often spread across society. However, a NACE International study released in 2002 estimates indirect costs to be, at the very least, equal to the direct costs of corrosion – an alarming revelation, given the same report estimated the direct costs of corrosion in America to be $276 billion, or 3.1% of the United States GDP at the time.[1] In confirmation of this work, a more recent study examined the global impact of corrosion and estimated the costs to be 3.4% of the global GDP.[2] Assuming similar projections and adjusting for inflation, the overall cost of corrosion (direct and indirect) in America today would total over $1 trillion. These figures highlight the extraordinary economic impact corrosion has in society, and more than justify the academic attention given to corrosion-related studies.

Corrosion is an electrochemical reaction, with coupled oxidation and reduction half-cell reactions, frequently referred to as anodic and cathodic reactions, respectively. In the most general example, the metal is oxidized, in a process analogous to the following anodic reaction:

$$\mathrm{M} \rightarrow \mathrm{M}^{n+} + ne^{-} \qquad \text{(Eq. 1)}$$

where *n* is the valence of the metal, indicating how many electrons are released during the reaction. As metal ions are released into solution, the metal surface becomes corroded and the bulk mass is reduced. The physical locations on the substrate surface of metal dissolution, where oxidation occurs, are known as anodic sites, or anodes, whereas the sites of reduction on the metal surface are known as cathodes.

Electrons generated by the anodic reaction make their way through the metal substrate and into the electrolyte by participating in reduction reactions at cathodic sites on the metal surface. These coupled cathodic reactions may take on several forms, depending on the surrounding conditions, namely solution pH and the availability of reactants.[3,4] Typically, hydrogen evolution or dissolved oxygen reduction, or a combination thereof, will ensue, as shown in the equations below:

$$2H^+ + 2e^- \rightarrow H_2 \qquad \text{(acidic solutions)} \qquad \text{(Eq. 2)}$$

$$2H_2O + 2e^- \rightarrow H_2 + OH^- \qquad \text{(neutral/alkaline solutions)} \qquad \text{(Eq. 3)}$$

$$O_2 + 4H^+ + 4e^- \rightarrow 2H_2O \qquad \text{(acidic solutions)} \qquad \text{(Eq. 4)}$$

$$O_2 + 2H_2O + 4e^- \rightarrow 4OH^- \qquad \text{(neutral/alkaline solutions)} \qquad \text{(Eq. 5)}$$

In order for corrosion reactions to take place, several environmental conditions must be met. First there must be an anodic reaction that generates electrons and a cathodic reaction taking place that accepts these electrons, as described above. Secondly, a conductive (metallic) path between the anodic and cathodic sites is required for the flow of electrons generated – this is typically fulfilled by the metallic substrate itself, as the anodic and cathodic reaction sites often lie on the same surface. Lastly, an electrolyte, or ionic pathway, is necessary to complete the electric circuit –this electrolyte also provides the bulk source of reactant for the cathodic reaction and actively enables metal dissolution at the anode to continue. Figure 1.1 illustrates general corrosion

of a steel surface with oxygen reduction serving as the main cathodic process – a situation that dominates under neutral or basic conditions.

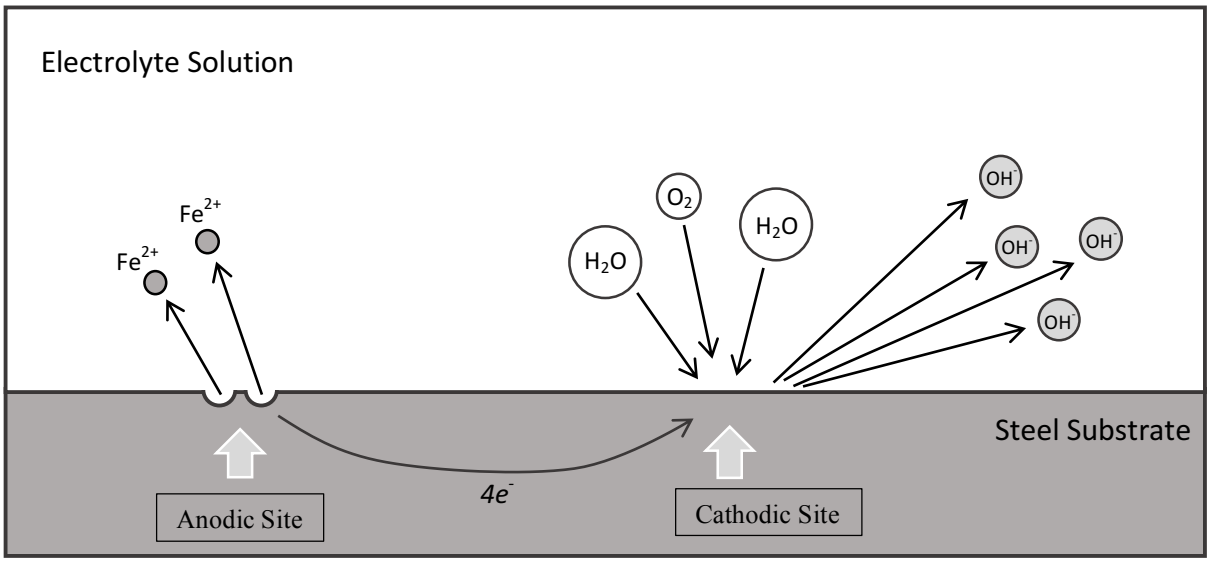

Figure 1.1. General corrosion process of steel substrate in electrolyte.

1.2. Corrosion of Steel

Carbon steels are an extremely ubiquitous building material, owing mainly to the abundance of available iron ore and its relatively low cost in comparison to replacement materials. Carbon steels are iron alloys with various amounts of carbon content, ranging from 0.05% to just upwards of 1%; they also contain other alloying elements, generally incorporated to improve mechanical properties. It is a versatile building material suitable for many applications because hardness and strength properties are easily tailored through alloying and heat treatment. As a result, carbon steel holds a large market share in the global economy, therefore it is important to understand the types of corrosion processes that impact carbon steels.

Carbon steel undergoes general corrosion, commonly termed *rusting*, when exposed to moisture. Steel rusting is one of the most pervasive and evident corrosion examples that is recognized by most individuals, as it results in a characteristic red-brown, solid powder staining

the steel surface. As previously highlighted in Figure 1.1, the corrosion of steel under basic conditions is modeled by the following half-cell reactions:

Anode: $2[\mathrm{Fe} \rightarrow \mathrm{Fe}^{2+} + 2e^{-}]$ (Eq. 6)

Cathode: $\mathrm{O_2} + 2\mathrm{H_2O} + 4e^{-} \rightarrow 4\mathrm{OH}^{-}$ (Eq. 5)

which can be combined into the overall corrosion reaction:

Overall: $2\mathrm{Fe} + \mathrm{O_2} + 2\mathrm{H_2O} \rightarrow 2\mathrm{Fe}^{2+} + 4\mathrm{OH}^{-}$ (Eq. 7)

The alkaline reduction of water in the absence of oxygen, represented in Eq. 3, requires a sufficiently negative potential to occur; instead the reaction in Eq. 5 predominates in most circumstances and is shown here. The Fe^{2+} ions released at the anode are fairly unstable, typically undergoing further reactions with oxygen and water from the surrounding environment to form various hydrated iron oxides, the most common of which is iron(III) oxide, or rust. Several intermediate reactions occur in the formation of rust, including the formation and subsequent reaction of iron hydroxides.[5] The following equations highlight some of the reaction pathways that result in the formation of iron hydroxides:

$$\mathrm{Fe}^{2+} + 2\mathrm{OH}^{-} \rightarrow \mathrm{Fe(OH)_2} \quad \text{(Eq. 8)}$$

$$2\mathrm{Fe(OH)_2} + \mathrm{H_2O} + \frac{1}{2}\mathrm{O_2} \rightarrow 2\mathrm{Fe(OH)_3} \quad \text{(Eq. 9)}$$

$$\mathrm{Fe} + 2\mathrm{H_2O} \rightarrow \mathrm{Fe(OH)_2} + 2\mathrm{H}^{+} \quad \text{(Eq. 10)}$$

Atmospheric corrosion of exposed mild steel proceeds under conditions with even the slightest amount of humidity. This is mainly due to the inability of mild steel to form a stable and protective oxide layer under mildly oxidizing conditions. One oddly beneficial side-effect of this is that a large part of the surface typically remains available for corrosion. This seems counterintuitive, but it can actually be an advantage – having more exposed surface area distributes the anodic current over a larger area, thereby reducing corrosion current density and overall

penetration rates. This type of corrosion is known as uniform corrosion; uniform corrosion is often the most preferable type of corrosion mechanism as it results in the lowest penetration rate, due to the metallic dissolution being distributed over the entire surface of the metal structure. Uniform corrosion occurs when the steel is of uniform composition and the whole surface is exposed to the same corrosive environment, however there are still certain settings where localized corrosion mechanisms are favored on mild steel surfaces.

As the name implies, localized corrosion is limited to a much smaller surface area than uniform corrosion, usually yielding significantly higher penetration rates. Consequently, localized corrosion processes, such as crevice corrosion, pitting, stress corrosion cracking, and galvanic corrosion, are more dangerous in terms of their failure mechanisms when compared to uniform corrosion. Therefore, understanding the causes and conditions of localized corrosion mechanisms is important so future design strategies may be implemented in order to prevent their manifestation. Crevice corrosion occurs within isolated volumes that are saturated with solution on the carbon steel surface. Typically, stagnant electrolyte conditions occur within the crevice and a progressively corrosive anodic environment arises, with the surrounding surfaces functioning as the cathode. These crevices are common under fastening joints on the steel where two surfaces adjoin each other. Bolts, rivets and washers are also favorable locations for crevice corrosion, especially if they are loosely tightened.[4]

In general, stress corrosion cracking (SCC) is caused by a combination of low tensile stresses on the substrate and exposure to particular chemicals that interact specifically with the alloy. SCC in steel is commonly associated with exposure to nitrates, ammonia, hydrogen gas, hydrogen sulfides or alkali hydroxides.[3,6]

Galvanic corrosion occurs when two dissimilar metals are physically joined and exposed to conductive electrolyte. This is because each alloy has a different corrosion potential and will impart a potential difference when coupled together. If sufficiently large, the potential difference will drive electrons from the more active metal to the less active metal, setting up a galvanic corrosion cell in the immediate vicinity of the metal-metal interface.[3,4] Carbon steel suffers from galvanic corrosion quite regularly, as bolts and fasteners attached to the substrate are typically machined of a different alloy, usually stainless steels, brass, copper, bronze or titanium. Because carbon steel (E_{corr} = -600 to -700 mV vs. SCE) has a more active corrosion potential than any of these other alloys (E_{corr} = 0.0 to -400 mV vs. SCE), the carbon steel will preferentially corrode. Figure 1.2 depicts a vivid example of this type of corrosion. Inert spacers at joints or insulating the two metals from one another is a standard method of preventing galvanic coupling and subsequent corrosion.

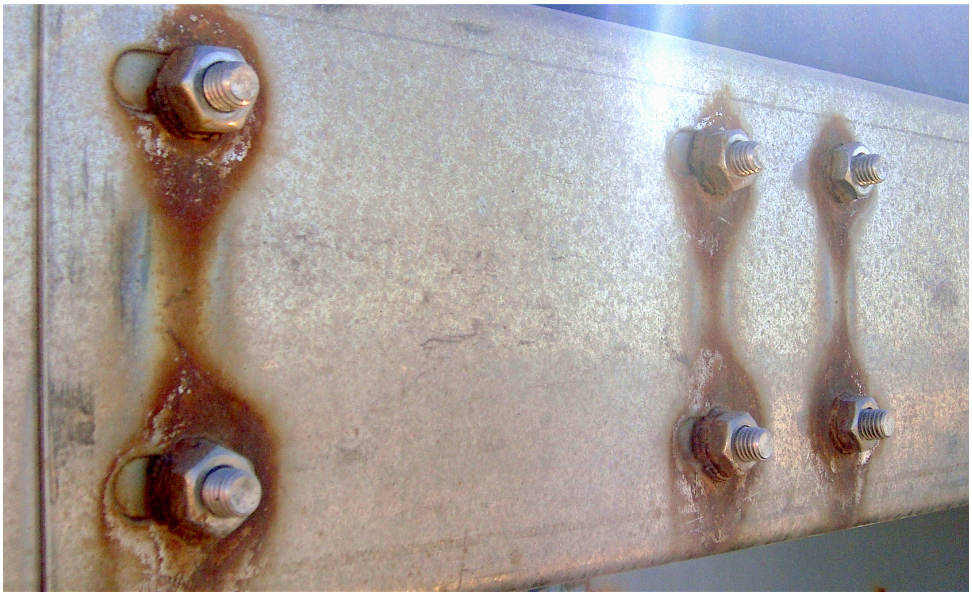

Figure 1.2. Galvanic corrosion of mild steel coupled with stainless steel nuts and bolts.

The corrosion of mild steel in hydrochloric acid is a special case that is increasingly encountered as industrial practices with acid solutions continue to expand; acid pickling and descaling, industrial cleaning and petrochemical processes are chief applications that have seen an increase in the use of acid solutions. It has therefore become necessary to investigate the interaction of steels with acids from both an academic and industrial perspective. As mentioned previously, cathodic reactions on the steel surface typically come in the form of hydrogen evolution or oxygen reduction, depending on solution pH and availability of dissolved reactants. Under aerated acidic conditions where H^+ ions and dissolved oxygen are available, both cathodic reactions occur, leading to larger cathodic currents than would otherwise be observed.[4] To counteract the polarization that results from higher cathodic activity, the anodic metal dissolution will proceed at an increased rate in order to supply the necessary electrons to the cathode, leading to elevated corrosion rates. Furthermore, concentration polarization limits associated with H^+ concentration are less pronounced because at lower pH there is a greater availability of this reactant for cathodic hydrogen evolution. The oxidation and reduction half-reactions occurring on the steel surface in hydrochloric acid can be described by the following:

Anode: $\mathrm{Fe} \rightarrow \mathrm{Fe}^{2+} + e^-$ (Eq. 6)

Cathode: $2\mathrm{H}^+ + 2e^- \rightarrow \mathrm{H}_2$ (Eq. 2)

Cathode: $\mathrm{O}_2 + 4\mathrm{H}^+ + 4e^- \rightarrow 2\mathrm{H}_2\mathrm{O}$ (Eq. 4)

Combining into the overall, unbalanced, corrosion reaction:

Overall: $\mathrm{Fe} + \mathrm{H}^+ + \mathrm{O}_2 \rightarrow \mathrm{Fe}^{2+} + \mathrm{H}_2 + \mathrm{H}_2\mathrm{O}$ (Eq. 11)

As seen, the overall reaction generates hydrogen gas and dissolved Fe^{2+} ions. The Fe^{2+} ions are free to react further with dissolved Cl^- ions or oxygen molecules in solution, forming ferrous chloride, $FeCl_2$, or iron oxides (Eq. 8-10). The depletion of H^+ ions goes largely unnoticed in large

quantities of solution, and concentration polarization is generally not appreciable, especially if there is sufficient solution mixing. However, in small solution quantities, such as a thin electrolyte film or stagnant electrolyte within pits or crevices, the local pH changes more easily and can have significant effects on the corrosion reaction.

1.3. Corrosion Prevention Strategies

The effects of corrosion, although ultimately inevitable, can be curtailed through various prevention strategies – several of which include the implementation of effective design approaches, coatings, cathodic protection, and corrosion inhibitors. One of the most important, yet often overlooked, methods of preventing corrosion occurs in the initial planning stages – proper design and collaboration between materials scientists and engineers during development can alleviate the emergence of many corrosion-prone situations. As suggested by Liss in *Corrosion Engineering Handbook*, several things to consider during the design stages include alloy selection, cost of replacement, avoiding galvanic and crevice corrosion situations, the operating environment and contamination concerns for process streams.[6] This process can be quite involved, however, planning and evaluating design strategies on the front end can reduce the need for costly repairs or maintenance expenses later. These concepts, while relevant in all aspects of modern manufacturing and construction, are especially important for structures and products intended to remain in service for many years, such as buildings, bridges, water and chemical treatment facilities, pipelines, storage tanks and other industrial or manufacturing plants.[4,6,7]

Perhaps the most common corrosion prevention strategy is the use of paints and coatings. Coatings provide some of the most cost effective and easily implemented strategies to preventing corrosion and extending the lifetime of substrates; coatings function by forming a physical barrier between the substrate and environment, effectively insulating the metal from the electrochemical

corrosion process that would occur if the substrates were exposed to electrolyte solutions or the atmosphere. Suitable coating selection and proper application techniques greatly impact corrosion prevention performance by promoting a well-adhered and continuous barrier. Additionally, substrate cleaning and preparation is equally important because dust, dirt, oil and other debris lead to imperfections in the coating upon curing. These imperfections create pathways for electrolyte to reach the substrate, enabling the formation of small corrosion cells, which can lead to pitting corrosion or further delamination of the coating around the defects as corrosion products form at the coating-substrate interface.[8] Furthermore, coatings utilized in high moisture environments will experience water adsorption over time, even coatings with excellent water barrier properties such as epoxies and polyurethanes; water penetration also provides a conductive path to the metal substrate. However, corrosion will only take place at these sites if cathodic reactants can also penetrate the coating thickness, or if they were trapped there initially upon coating application.

It is important to remember that even impeccably applied coating systems will fail eventually. Degradation due to mechanical abrasion, thermal fluctuations or radiation will predominate over time on surfaces that are not routinely inspected and repaired, leading to bare metal exposure and subsequent corrosion. It is for this reason that further protection strategies, such as cathodic protection and corrosion inhibitor additives, are often utilized in conjunction with coating systems.

Cathodic protection is a common corrosion mitigation technique that is based on galvanic principles of anodic and cathodic behavior. The same electrochemical processes that occur in a galvanic cell are taken advantage of in order to protect a specific metal substrate. When two dissimilar metals are in electrical contact with each other, and exposed to a conductive electrolyte, corrosion of the more active metal typically occurs. The process mirrors that of a standard galvanic

cell in which the more active metal corrodes, releasing metal ions and generating electrons, while the less active (more noble) metal is protected as the cathode. A metal's activity is depicted on the galvanic series (Figure 1.3), with relative positions indicating whether the coupled metals will function as the cathode or anode in a given electrochemical setup. For example, if zinc and carbon steel are coupled to one another, zinc will corrode, but if carbon steel and copper are coupled, the carbon steel will corrode. This behavior can be directly correlated to carbon steel's relative position on the galvanic series in relation to zinc and copper.[4,6]

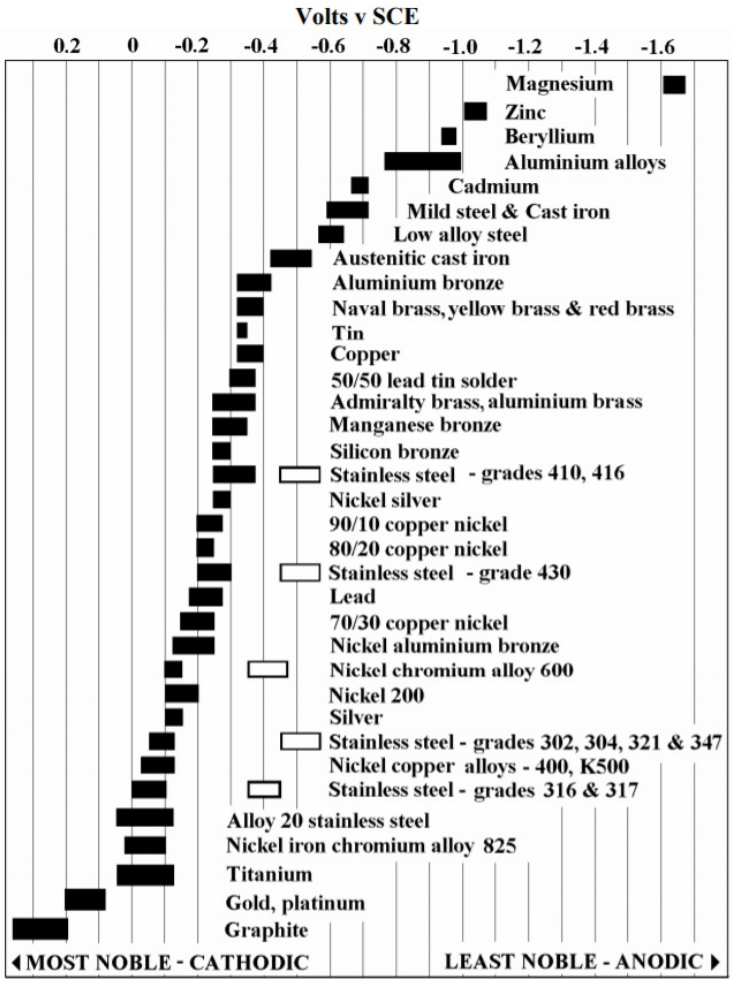

Figure 1.3. The galvanic series.[9]

An important distinction with galvanic coupling is that the anodic and cathodic sites are on different metal substrates, and predicting which metal will be the anode and which the cathode is relatively easy. This has allowed engineers to come up with better design strategies that avoid galvanic coupling situations entirely, or actually use the phenomenon as a corrosion mitigation technique, as described below with sacrificial anodes.

The use of sacrificial anodes takes advantage of the difference in metal activity in order to protect the less active metal substrate. A metal that has high activity in the galvanic series is coupled to a metal of lesser activity that is to be protected, either through direct contact or with an external wire. This practice forces the metal structure into a cathodic role, protecting it from corrosion, while the active metal functions as the corroding anode. For this reason, sacrificial anodes are typically made of zinc- or magnesium-based alloys, as they are two of the highest activity metals in the galvanic series. For example, since the 19th century, steel ship hulls have been regularly equipped with large blocks of zinc, effectively creating a galvanic cell between the steel, zinc and sea water. In this galvanic cell, the zinc blocks are depleted slowly by the anodic reaction while the steel operates as the cathode, protecting it from attack by the seawater. This is also the same principle behind galvanizing iron and steel with a zinc surface or utilizing zinc- and magnesium-rich primers for coating applications.[3,6,10] Sacrificial anodes function by providing electrons to the cathode, promoting relatively harmless reduction at its surface, rather than destructive oxidation. This protection will continue until the anode is fully consumed and the current to the cathode disappears, which is why fully-depleted sacrificial anodes should be replaced immediately.

In an alternative form of cathodic protection, an impressed current on the system can also serve to perpetuate the cathodic reaction on the substance needing protection. This method replaces

the metallic source of electrons observed in the sacrificial anode system with an impressed direct current from a power source. The supply of electrons provided by the impressed current forces the substrate into a cathodic role, protecting it from oxidation by the surrounding environment. Buried steel pipelines and tanks are often protected by this method[4,6,11].

Another practical corrosion mitigation technique, and the focus of this work, is the use of corrosion inhibitors. Inhibitors can be used as a standalone method or used in conjunction with previously discussed techniques. Specifically, inhibitors are additives that can be incorporated into process streams, added to coating formulations or applied as a pretreatment to substrates.

1.4. Corrosion Inhibitors

Corrosion inhibitors are molecules that, when used in small quantities, enhance an electrochemical system's resistance to corrosion or reduce the corrosivity of the environment. Inhibitors are a cost-effective, corrosion mitigation strategy that find heavy use in industrial applications, especially crude oil extraction and refining processes, water treatment, circulation and cooling infrastructures, and many manufacturing processes that utilize solution baths and transport.

Inhibitor molecules can be organic or inorganic and often are proprietary in nature, sometimes creating difficulties in elucidating their complex interactions with electrochemical systems. In general, however, inhibitors function by impacting some part of the corrosion reaction as described:

Anodic inhibitors – suppress the anodic dissolution reaction

Cathodic inhibitors – suppress the cathodic reduction reactions

Mixed-type inhibitors – suppress both anodic and cathodic reactions

Determining the specific mechanism by which each inhibitor compound reduces corrosion reaction rates is an important aspect for deciding possible applications. Although there is no comprehensive theory to explain inhibitor effects or predict inhibitor performance, progressive advances in research have enabled faster and more-reliable testing of inhibitor systems. Generally, molecular structure of the inhibitor can hint at its functionality, but further investigation is always necessary. Mechanistic characterization can be performed through various electrochemical tests and surface characterization techniques, as investigated later in the present work. Additionally, some researchers have studied electrolyte compositions to see if inhibitor molecules are capable of complexing with corrosion products, such as metal ions or metal oxides, or other dissolved species.[12–14] These investigative methods may give insight into secondary inhibition mechanisms that may help explain synergistic effects or shed light on why inhibitors of similar molecular structure have significantly different inhibitive performance.

There are several ways in which to classify inhibitors, and some classifications undoubtedly overlap, but generally the most common method of classification is by inhibitor function. Most, if not all, corrosion inhibitors fall into one or more of the following categories:

1. Environmental scavengers
2. Passivating inhibitors
3. Precipitation inhibitors
4. Vapor phase inhibitors
5. Organic inhibitors

Environmental scavengers interfere with the corrosion reaction by interacting with species present in the electrolyte – by far the most common being oxygen scavengers. Oxygen scavengers sequester dissolved oxygen, lowering its concentration and availability to the cathode for the

corrosion reduction reaction. Sodium and potassium sulfates and sulfites, as well as hydrazine, are additives that can be incorporated into deaerated water systems, significantly reducing oxygen content. Oxygen scavengers work well in corrosive environments where the cathodic reaction is controlled by the reduction of oxygen, but have little effect in acidic environments where hydrogen evolution predominates.[15] In such situations, antimony and arsenic ions have been effective at slowing the cathodic hydrogen evolution reaction.[5] In some heat exchange systems where dissolved CO_2 creates a mildly acidic environment, aliphatic amines are occasionally added in order to neutralize the solution, effectively reducing the H^+ concentration and lowering the rate of the hydrogen evolution cathodic reaction. The same methodology is also utilized in some oil refining process where acidic conditions, due to the presence of hydrogen sulfide in oil, arise.[4]

Passivating inhibitors are some of the most effective and widely used substances for corrosion prevention. As their name suggests, they function by forcing the metallic substrate into the passive state. As mentioned previously, the passivation state is a potential range beyond the active state where a reduction in corrosion currents are observed, and is attributed to the formation of a protective oxide layer. Passivating inhibitors are oxidizing substances that shift the substrate to potentials within its passivation range, promoting the formation of this oxide layer. Recall that mild steels generally do not form a sufficiently protective oxide layer on their own, however in the presence of passivating inhibitors, such as chromates ($CrO_4{}^{2-}$) or nitrites ($NO_2{}^-$), a stable oxide layer that offers significantly improved protection is readily formed.

Chromates favor adsorption to the substrate in the presence of dissolved oxygen, while the nitrite ion is capable of coordinating to the metallic surface in several different geometries. In either case, a protective complex that covers the surface is formed.[6] Due to the severe toxicity of hexavalent chromium, though, chromates are usually limited to closed-loop systems, and are

slowly being phased out as a result of stricter environmental policies. Several other passivating inhibitors include molybdate, silicate, phosphate, borate and tungstate. Great care must be taken when monitoring systems that utilize passivating inhibitors because insufficient concentrations can lead to incomplete surface passivation; this tends to accelerate the rate of corrosion leading to pitting at unprotected sites.[3,4,6]

As their name implies, precipitation inhibitors are substances that promote the formation of precipitates on the substrate surface, providing a protective barrier to the electrolyte solution. Ca^{2+} and Mg^{2+} ions are sometimes considered precipitation inhibitors, as their presence in hard waters has a tendency of forming carbonate salts that precipitate on the metal surface and form a protective layer. These two ions are sometimes referred to as cathodic inhibitors, because they precipitate preferentially at cathodic sites where local OH^- concentrations are higher.[4] Phosphate and zinc salts are also commonly used precipitation inhibitors.[6] In a study performed by Veldman and Trahan, a reduction in corrosion rate was observed through the use of quinone in the presence of alkanolamines, commonly seen in natural gas processing. The inhibition was attributed to the reduction of iron ions in solution to the stable magnetite iron oxide, precipitating on the substrate surface and forming a protective layer.[16]

It is widely accepted that the corrosion inhibition offered by organic inhibitors is primarily due to these molecules being adsorbed onto the metallic surface, forming a thin protective film. As alluded to earlier, surface adsorption mechanisms are correlated to mixed-type inhibition, as both anodic dissolution sites and cathodic reaction centers are protected; numerous studies have confirmed this trend.[3,4,17–23] General corrosion texts suggest that organic inhibitor function can be improved with larger molecular size and weight, as well as a higher electron density – indeed, research in the last decade has focused specifically on the last aspect, with researchers studying

the effects of molecules incorporating heteroatoms, such as nitrogen, sulfur and oxygen, into ring structures. These studies have shown corrosion inhibition efficiencies to be greatly improved by molecules with these electronic structures, with the adsorption of the organic molecules being largely attributed to the localized electron densities offered by these heteroatoms, enabling them to interact with the surface, either through electrostatic forces due to a charged metallic surface, or through a coordination mechanism in which electronic structures are shared between the inhibitor and metallic substrate.[6,17,18,21,22,24–27]

Improved surface coverage (θ) on the metallic surface is directly related to improved corrosion inhibition, as a more uniform and stable adsorptive layer serves as a better barrier to the aggressive electrolyte solution. In fact, inhibitor efficiency is a good indicator of the extent of surface adsorption. Thus, inhibitor performance is often expressed in terms of inhibitor efficiency (%IE), which is typically calculated from Eq. 12:

$$\%IE = \frac{i_o - i}{i_o} \cdot 100 \qquad \text{(Eq. 12)}$$

where i_o and i are corrosion current densities measured in the absence and presence of inhibitor, respectively. Other parameters related to i_o are sometimes substituted into the equation instead.

Inhibitor selection for any variety of applications is influenced by several factors, including effectiveness, feasibility, cost and toxicity. In many situations, the most efficient inhibitors for a given situation are not cost-effective, as is often the case in single pass solution systems, like pipeline infrastructures. Furthermore, some systems, such as potable water treatment facilities, are unable to use effective inhibitors, such as chromates, due to the public health concerns involved. Finding a balance between all of these influences is challenging, which is why continued development of inhibitor systems, especially of the non-toxic, organic variety, is expected to continue. Indeed, over the last two decades, there has been a significant surge in corrosion inhibitor

research associated with organic, non-toxic substances. These reviews offer excellent sources for discussion of organic inhibitor studies.[28–38] Although this work investigates the corrosion inhibition effects of non-toxic, organic inhibitors on mild steel, the focus is on developing a consistent electrochemical and surface characterization method to study these molecules.

1.5. References

(1) Koch, G. H.; Brongers, M. P. H.; Thompson, N. G.; Virmani, Y. P.; Payer, J. H. *Corrosion costs and preventive strategies in the United States*; 2002.

(2) Koch, G.; Varney, J.; Thompson, N.; Moghissi, O.; Gould, M.; Payer, J. *International Measures of Prevention, Application, and Economics of Corrosion Technologies Study*; 2016.

(3) McCafferty, E. *Introduction to Corrosion Science*; 2010.

(4) Jones, D. A. *Principles and Prevention of Corrosion*, 2nd ed.; Prentice Hall: Upper Saddle River, NJ, 1996.

(5) Fontana, M. G. *Corrosion engineering*, 3rd ed.; McGraw-Hill: New York, 1986.

(6) *Corrosion Engineering Handbook*; Schweitzer, P. A., Ed.; Marcel Dekker, Inc., 1996; Vol. 1.

(7) Manahan, S. E. *Industrial ecology: Environmental chemistry and hazardous waste*; Lewis Publishers, 1999.

(8) Osswald, T. A.; Menges, G. *Material science of polymers for engineers*, 3rd ed.; Hanser Publications: Cincinnati, OH, 2010.

(9) Atlas Steels. *Atlas Tech Note No. 7*; 2010.

(10) Bierwagen, G.; Battocchi, D.; Simões, A.; Stamness, A.; Tallman, D. *Prog. Org. Coatings* **2007**, *59* (3), 172–178.

(11) Popoola, L.; Grema, A.; Latinwo, G.; Gutti, B.; Balogun, A. *Int. J. Ind. Chem.* **2013**, *4* (1), 35.

(12) Amin, M. A.; Khaled, K. F.; Fadl-Allah, S. A. *Corros. Sci.* **2010**, *52* (1), 140–151.

(13) Amin, M. A.; Ahmed, M. A.; Arida, H. A.; Arslan, T.; Saracoglu, M.; Kandemirli, F. *Corros. Sci.* **2011**, *53*, 540–548.

(14) Ogle, K.; Weber, S. **2000**, *147* (5), 1770–1780.

(15) Cavano, R. R. *Sulfites for oxygen control*; 2007.

(16) Veldman, R. R.; Trahan, D. O. *Fuel Energy Abstr.* **2000**, *41* (3), 144.

(17) Elbelghiti, M.; Karzazi, Y.; Dafali, A.; Hammouti, B.; Bentiss, F.; Obot, I. B.; Bahadur, I.; Ebenso, E. E. *J. Mol. Liq.* **2016**, *218*, 281–293.

(18) Solmaz, R. *Corros. Sci.* **2014**, *79*, 169–176.

(19) Afia, L.; Salghi, R.; Benali, O.; Jodeh, S.; Warad, I.; Ebenso, E.; Hammouti, B. *Port. Electrochim. Acta* **2015**, *33* (3), 137–152.

(20) Bozorg, M.; Shahrabi Farahani, T.; Neshati, J.; Chaghazardi, Z.; Mohammadi Ziarani, G. *Ind. Eng. Chem. Res.* **2014**, *53* (11), 4295–4303.

(21) Tourabi, M.; Nohair, K.; Traisnel, M.; Jama, C.; Bentiss, F. *Corros. Sci.* **2013**, *75*, 123–133.

(22) Raja, P. B.; Qureshi, A. K.; Abdul Rahim, A.; Osman, H.; Awang, K. *Corros. Sci.* **2013**, *69*, 292–301.

(23) Al-Otaibi, M. S.; Al-Mayouf, A. M.; Khan, M.; Mousa, A. A.; Al-Mazroa, S. A.; Alkhathlan, H. Z. *Arab. J. Chem.* **2014**, *7*, 340–346.

(24) Ashhari, S.; Sarabi, A. A. *Surf. Interface Anal.* **2015**, *47* (2), 278–283.

(25) Yang, D. Corrosion inhibition performance of imidazolium ionic liquids and their influences on surface ferrous carbonate layer formation, 2016.

(26) Kaya, S.; Tüzün, B.; Kaya, C.; Obot, I. B. *J. Taiwan Inst. Chem. Eng.* **2016**, *58*, 528–535.

(27) Hu, J.; Huang, D.; Zhang, G.; Song, G. L.; Guo, X. *Corros. Sci.* **2012**, *63*, 367–378.

(28) Sanyal, B. *Prog. Org. Coatings* **1981**, *9* (2), 165–236.

(29) Raja, P. B.; Sethuraman, M. G. *Mater. Lett.* **2008**, *62* (1), 113–116.

(30) Mo, S.; Luo, H. Q.; Li, N. B. *Chem. Pap.* **2016**, *70* (9), 1131–1143.

(31) Chigondo, M.; Chigondo, F. *J. Chem.* **2016**, *2016*.

(32) Sangeetha, M.; Rajendran, S.; Sathiyabama, J.; Krishnavenic, A. *Port. Electrochim. Acta* **2013**, *31* (1), 41–52.

(33) Gece, G. *Corros. Sci.* **2011**, *53* (12), 3873–3898.

(34) Xhanari, K.; Finšgar, M. *RSC Adv.* **2016**, *6*, 62833–62857.

(35) Sharma, S. K.; Peter, A.; Obot, I. B. *J. Anal. Sci. Technol.* **2015**, *6* (1), 26.

(36) Swathi, P. N.; Rasheeda, K.; Samshuddin, S.; Alva, V. D. P. *J. Asian Sci. Res.* **2017**, *7* (8), 301–308.

(37) Umoren, S. A.; Solomon, M. M. *J. Environ. Chem. Eng.* **2017**, *5* (1), 246–273.

(38) Myrdal, R. *Corrosion Inhibitors – State of the art*; 2010.

CHAPTER 2. ELECTROCHEMICAL CHARACTERIZATION PROCEDURE FOR ORGANIC MOLECULES AS CORROSION INHIBITORS ON MILD STEEL

2.1. Abstract

The corrosion inhibition ability of some organic molecules, including 3,4-dihydroxyphenylacetic acid (DOPAC), 4-aminosalicylic acid, 5-aminosalicylic acid, adrenalone, allantoin, betaine (trimethylglycine), diazolidinyl urea, and dopamine, was investigated on steel in aqueous solutions using a set of electrochemical characterization methods, including open circuit potential (OCP) monitoring, potentiodynamic scanning (PDS), linear polarization resistance testing (LPR), and electrochemical impedance spectroscopy (EIS), with the goal of establishing a consistent screening and characterization method. An initial study of inhibitor effectiveness on mild steel under 3.5% (w/v) NaCl electrolyte conditions using LPR was performed in order to screen the original eight candidate inhibitors to just three molecules for further investigation in a process sometimes termed hereafter as "down-selection".

The initial PDS investigation resulted in similar anodic and cathodic Tafel constants for each inhibitor system, regardless of molecular structure, suggesting that estimating these values with LPR analysis is acceptable. The LPR investigation in 3.5% NaCl resulted with DOPAC, adrenalone, and dopamine each demonstrating significantly lower corrosion rates than the other candidate molecules at comparable concentrations and time scales. The order of inhibition performance at 10 mM concentration after 14 days of inhibitor exposure was adrenalone > dopamine > DOPAC, at 58.3%, 57.6% and 52.8% inhibition efficiency, respectively. The other inhibitors showed milder inhibitive properties in comparison. All inhibitors, except betaine, displayed improved performance with increasing concentration, even if only slightly. The lower

concentrations investigated for 5-aminosalicylic acid, adrenalone and dopamine resulted in higher corrosion rates, suggesting incomplete surface coverage of the substrate.

Further LPR investigations of the down-selected inhibitors in acidic media revealed that the trends seen in 3.5% (w/v) NaCl are similar. While corrosion rates did increase in the aggressive electrolyte, their inhibition efficiencies were much higher, when compared to the uninhibited solutions in either electrolyte. Inhibitor performance tended to improve with increasing concentration, reaching inhibition efficiencies of 85.6% for DOPAC, 89.6% for adrenalone and 90.4% for dopamine. The overall method demonstrates a useful screening and characterization procedure for continued investigation of future inhibitor systems.

2.2. Experimental

2.2.1. Substrate and Inhibitor Solution Preparation

Carbon steel test panels were obtained from Q-Lab Corporation, SAE 1008 carbon steel panels (refer to Table 2.1) measuring 76 mm x 152 mm and 0.8 mm thick. The test panels were degreased with acetone and then stored in a desiccator to help achieve low moisture conditions until panels were needed. Prior to experimentation, the steel substrates were sanded with 400-grit silicon carbide sandpaper and placed under a stream of nitrogen gas to remove any sanding debris. Then the panels were masked with tape, made from a polyester backing and a silicone adhesive, to seal off an exposed testing area of 1 cm^2. Immediately prior to applying the inhibitor solutions, another acetone rinse was performed, followed by drying under a stream of N_2 gas.

Table 2.1. Elemental composition of SAE 1008 steel used for all substrates in this work. The equivalent weight is 27.92.[1]

Element	Composition (%)
Iron	99+
Manganese	0.6 max
Carbon	0.15 max
Phosphorus	0.03 max
Sulfur	0.035 max

Two types of corrosion-inducing electrolytes were used for the electrochemical characterization tests – 3.5% (w/v) sodium chloride and 1 M hydrochloric acid. Deionized, 18 MΩ, ultra-pure water was used to prepare both solutions in order to reduce undesirable, ionic contaminant influences on the electrochemical testing. All chemical inhibitors investigated (shown in Figure 2.1) were used as-received from Sigma-Aldrich to prepare stock solutions. They were dissolved directly in the corrosion-inducing media at specified concentrations for each type of electrochemical test. Additionally, alcohol-amine positive controls of ethanolamine (ETA) and triethanolamine (TEA) supplied by Sigma-Aldrich, as well as a commercial zinc phthalate anticorrosion additive called Heucorin FR, supplied by Heubach, were incorporated into the studies for comparison.

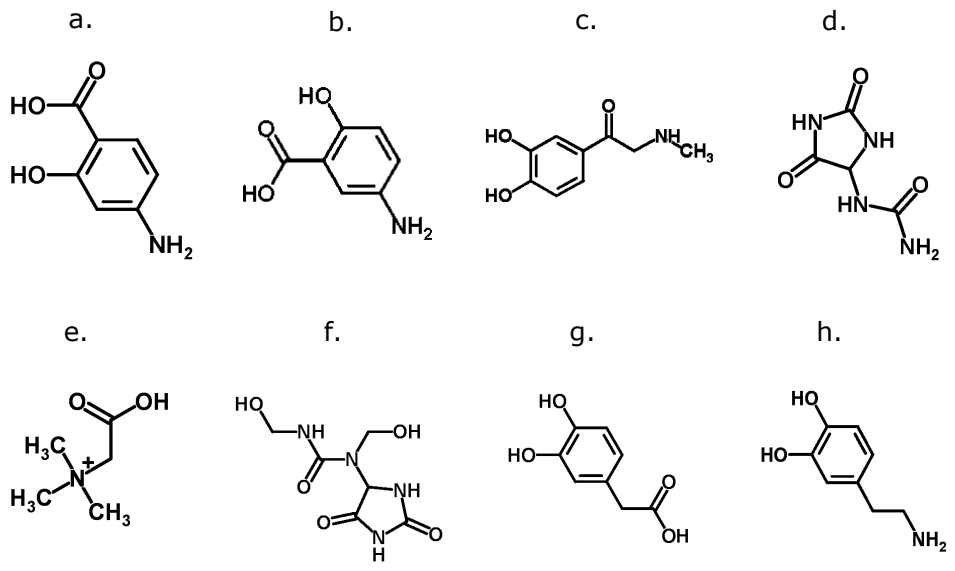

Figure 2.1. Schematic representation of the inhibitor molecules; (a) 4-aminosalicylic acid, (b) 5-aminosalicylic acid, (c) adrenalone, (d) allantoin, (e) betaine, (f) diazolidinyl urea, (g) 3,4-dihydroxyphenylacetic acid (DOPAC), (h) dopamine.

2.2.2. Electrochemical Techniques

Characterizing metallic substrate systems with electroanalytical techniques is an effective way to obtain important electrochemical information, allowing materials scientists to predict corrosion behavior reliably, without having to wait for long-term studies to be performed. One such set of methods involves the use of a potentiostat/galvanostat, an instrument that is capable of applying an electric signal and evaluating an electrochemical system's response. Potentiostatic techniques apply a potential to the system and measure the current response, whereas galvanostatic techniques apply a current and measure the potential response. This work utilizes the potentiostatic technique, performing potentiodynamic polarization, linear polarization resistance and electrochemical impedance spectroscopy tests.

Electrochemical characterizations were performed using a Gamry Instruments Reference 600 Potentiostat/Galvanostat/ZRA paired with Gamry Instruments Framework Data Acquisition

Software version 6.32. This software package includes the *DC105* software for potentiodynamic and linear polarization testing, as well as the *EIS300* software for electrochemical impedance spectroscopy testing. Additionally, Gamry Instruments' software, *Gamry Echem Analyst* version 6.21, was used for data analysis. A cylindrical glass corrosion cell was clamped to the flat steel substrate and sealed with an O-ring – this cell was then filled with the appropriate test solution. A three-electrode setup was used for all experiments; the steel substrate, with an exposed area of 1 cm^2, functioned as the working electrode, a saturated calomel electrode (SCE) was utilized as the reference electrode, and high surface-area platinum mesh served as the counter/auxiliary electrode. All potentials listed are measured against the SCE reference electrode unless otherwise stated. Figure 2.1 displays the general scheme of how tests were setup for each test.

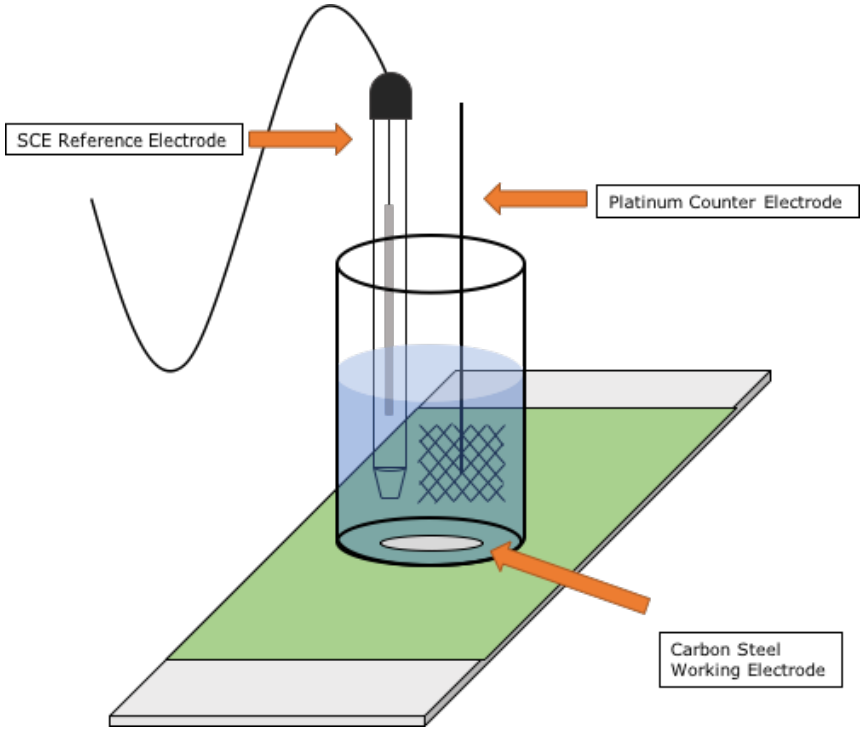

Figure 2.2. Depiction of the general three-electrode corrosion cell setup used in electrochemical characterization tests.

2.2.3. Open Circuit Potential (OCP)

The open circuit potential, sometimes referred to as corrosion potential (E_{corr}) or the steady-state potential, is defined as the electrochemical potential of the electrode at $I = 0$, where there is no net flow of electrons. In other words, E_{corr} is the potential where the rates of the system's anodic and cathodic reaction rates offset – a change in either half-reaction results in a shift in the steady-state potential. OCP drift of the electrochemical system does occur, but typically does so over much longer time scales, especially without any outside influence acting on the system.

Measuring OCP involves recording the potential (V) of an electrochemical system over time; once a stable value is established, that voltage is considered to be the steady-state potential of the system in its present environment. Electrode selection and condition, as well as solution composition will impact the steady-state potential, so determining E_{corr} under various influences, including the presence and absence of inhibitors, gives insight into the roles these conditions play on the corrosion potential of the system. A shift in equilibrium can be the result of adsorption of inhibitor molecules to the metal surface, the formation of an oxide layer or by changing solution conditions, such as solution velocity (stirring), temperature, or the addition/depletion of corrosion reactants, like dissolved oxygen or H^+, which also suggests a direct correlation to solution pH. Evaluating E_{corr} while varying these system characteristics can give insight into the corrosion mechanics occurring on the substrate surface.

For example, as described by the mixed potential theory, a shift in the corrosion potential to more positive (noble) values suggests an increase in the dominant anodic reaction rate or a decrease in the cathodic reaction rate.[2–4] Because the cathodic reaction is heavily dependent on the availability of H^+ and dissolved oxygen, a decrease in either might ultimately explain a shift in

E_{corr}. Indeed, for steel it is widely known that alkaline conditions correlate to lower corrosion rates, an effect of impeding the cathodic reaction due to low H^+ availability.[2,4–7]

In this work, long-term open circuit potential (OCP) testing was performed with and without the candidate inhibitors in order to determine the active corrosion potential of each inhibitor system. Concentrations of the inhibitors in 3.5% NaCl solution varied from 0.01 mM to 10 mM, depending on solubility of the chemical. The OCP was monitored for 18 hours at 0 mV/s stability, with measurements taken every 10 seconds.

2.2.4. Potentiodynamic Scanning (PDS)

Potentiodynamic scanning is an electroanalytical technique that allows for electrochemical processes at an electrode surface to be investigated. The method involves sweeping the potential (E) of the working electrode at a predetermined rate while recording the current (I) response of the system. The technique can be modified in terms of scanning rate and potential range in order to obtain mechanistic information about an electrochemical system, such as passivity behavior, corrosion potential, Tafel activity, pitting susceptibility, and even reduction reaction kinetics.[8] One such parameter is the potential range, which usually varies from around ± 100 mV vs. E_{corr} to upwards of ± 5 V vs. E_{corr}.

Polarizing a mild steel substrate a few hundred millivolts results in curves displaying Tafel behavior, linear regions associated with the anodic and cathodic reaction rates. Polarizing the substrate even more in the positive direction will reveal the active state, a region of larger current as the anodic reaction is favored. And still polarizing a little further will reveal a plateau of depressed current across several hundred millivolts of potential, known as the passive range. This is attributed to the formation of an oxide layer on the substrate that reduces the area of exposed substrate available for corrosion to take place. Some metals, such as aluminum and its alloys, have

easily recognizable passivation ranges with significant reductions in current. This is because aluminum readily oxidizes when exposed to oxygen, forming a uniform, compact oxide layer that offers excellent corrosion protection. Mild steels display similar passivating behavior; however, the oxide layer is much more porous, adheres poorly to the steel substrate, and is easily disturbed under mild agitation. Consequently, significantly less corrosion protection is offered and the current reduction in the passivation region of carbon steels is not nearly as pronounced as it is in aluminum. The behavior of a substrate's passive layer can be directly related to the current density displayed on the polarization curve, and the range over which it occurs. Scanning a sufficiently large range of potentials is crucial for observing the active and passive ranges, which is why understanding the substrate and selecting the appropriate test parameters for each electrochemical technique are important.

The PDS experimental parameters relating to scan range and scan rate varied through the length of this project in order to obtain different information relating to Tafel activity and passivation behavior. Tafel slopes can be extracted within a smaller potential range about E_{corr} (± 300 mV), so these scans were performed first in order to obtain the β_a and β_c Tafel constants, which are required for use during LPR analysis. After down-selection of the inhibitors, PDS scans that spanned a larger potential range were obtained in order to evaluate the passivation effects of the inhibitors. Passivation of mild steel occurs from about 0.5 V to upwards of 3 V, so this range was specifically included in the polarization range.

The first set of experiments was used as an initial screening process for the eight inhibitor candidates. These tests involved separate anodic and cathodic scans in 3.5% NaCl electrolyte; the measurements were made from the open circuit potential to +300 mV and -300 mV at a scan rate of 0.5 mV/s. Separate anodic and cathodic tests were performed in order to alleviate the large drift

observed between the open circuit value measured prior to the start of the experiment and the apparent E_{corr} measured during a typical single-scan experiment. The OCP drift is a result of the surface changing during the polarization measurements taken before the potential reaches E_{corr}. After the initial screening process, PDS scans were performed on the down-selected inhibitors in both 3.5% (w/v) NaCl and 1 M HCl from -1 V to 7 V and -1 V to 5 V (vs. E_{corr}), respectively. The polarization rates varied between 0.5 mV/s to 20 mV/s. Suggested by ASTM G5, an initial delay of 60 minutes was used in each set of experiments to allow the system sufficient time to establish a quasi-stable corrosion potential before polarization. The test parameters are summarized below, in Table 2.2.

Table 2.2. Testing parameters for potentiodynamic experiments. The partial scan parameters are from individual anodic and cathodic scans, prior to down-selection of inhibitor candidates in 3.5% NaCl. The full scans were performed on the down-selected inhibitors.

Test	3.5% NaCl - Partial Scan	3.5% NaCl – Full Scan	1 M HCl – Full Scan
Initial E (V) [vs. E_{corr}]	0	-1	-1
Final E (V) [vs. E_{corr}]	± 0.3	7	5
Scan Rate (mV/s)	0.5	0.5	5-20
Sample Period (s)	1	1	0.5
Sample Area (cm^2)	1	1	1
Density (g/cm^3)	7.87	7.87	7.87
Equivalent Weight	27.92	27.92	27.92
Initial Delay (s)	3600	3600	3600

2.2.5. Linear Polarization Resistance (LPR)

Linear polarization resistance (LPR) testing is a specialized polarization technique that helps elucidate reaction kinetics information at the working electrode. LPR is a rapid, non-destructive method primarily used for determining reliable corrosion rate data, making it an obvious asset for evaluating the efficiency of corrosion inhibitors. LPR, like PDS, involves measuring the current response as the potential is changed. The slope of the resultant polarization

curve is then used to determine polarization resistance (R_p), which is essentially a measure of how changes in potential impact the current. In an ideal setting with a high polarization resistance, the substrate-inhibitor system will display minimal change in current with large changes in potential.[8] In other words, the ideal system resists corrosion over a broader range of environmental conditions.

Fundamentally, the LPR experimental process is almost identical to PDS, except that the probed potential range is one or two orders of magnitude smaller – usually ± 10 – 30 mV vs. E_{corr}. One advantage of the reduced polarization range, when compared to PDS, is that the scan rate can be slower and still offer rapid data acquisition and the response is usually linear; this is significant because slower scan rates permit more time for the system to stabilize at each potential step, yielding more accurate current response data. Additionally, the current response, while still measurable, is much smaller because polarization is performed only within the immediate vicinity of E_{corr}; this has the effect of minimizing the electric current across the substrate, giving LPR its non-destructive quality.

Linear polarization resistance testing can trace its theoretical roots back to 1938, to a landmark corrosion science paper by Wagner and Traud,[9,10] in which they proposed that the slope of the polarization curve at its equilibrium state (E_{corr}) might be used to calculate the corresponding electrochemical reaction rate. In 1951, this theorized relationship was observed by scientists in the corrosion of various iron samples; the polarization term (R_p) was born out of this work.[11] It was suggested to have the following simple relationship:

$$R_p = \frac{\Delta E}{\Delta i} \qquad \text{(Eq. 13)}$$

By 1957, Stern and Geary had taken this relationship a step further and derived an equation relating the slope of a polarization curve (R_p) to the measured current density, i_{corr}, at values near

the system's steady-state potential, E_{corr}:

$$R_p = \frac{\Delta E}{\Delta \log(i_{\Delta E \to 0})} = \frac{B}{i_{corr}} \quad \text{(Eq. 14)}$$

where R_p is polarization resistance corrected for electrode area ($\Omega \cdot cm^2$), i_{corr} is the corrosion current density ($\mu A/cm^2$), and B is a proportionality constant for the given corrosion system defined by:

$$B = \frac{\beta_a \beta_c}{2.303(\beta_a + \beta_c)} \quad \text{(Eq. 15)}$$

where β_a and β_c are the anodic and cathodic Tafel constants. These values vary depending on local electrochemical environment parameters, including solution conditions and electrode composition. Eq. 14 and 15 can be combined into what is known as the Stern-Geary equation:[12]

$$i_{corr} = \frac{\beta_a \beta_c}{2.303 \cdot R_p(\beta_a + \beta_c)} = \frac{B}{R_p} \quad \text{(Eq. 16)}$$

This equation forms the theoretical basis for linear polarization resistance testing, in which i_{corr}, the term associated with reaction rate and the value necessary to establish corrosion rate, can be calculated from the experimentally-determined values R_p, β_a, and β_c.

Application of the Stern-Geary equation requires linearity of the polarization curve, hence the name of the technique and reason for scanning a sufficiently small potential range about E_{corr} in order to assure a linear current response when plotted. Unfortunately, due to the limited polarization range of LPR experiments and lack of data points that are sufficiently polarized from E_{corr}, Tafel constants cannot be easily extracted from LPR experiments. Instead, a separate PDS experiment using the same electrode material under duplicate conditions is often performed in order to determine β_a and β_c, a process that was utilized in this work. Alternatively, these values can be assumed or obtained from literature describing similar electrochemical systems, a widely-accepted practice.[13–16]

Linear polarization resistance, while offering less mechanistic information of the electrochemical system than a full potentiodynamic scan, has the advantage of quickly determining reliable corrosion rate data without destroying the substrate. This makes LPR particularly useful for in situ experiments where monitoring the mechanical integrity of metal structures, such as bridges, above- and below-ground pipelines and storage tanks, marine vessels and offshore drilling rigs, is of great importance for economic and safety purposes. In a laboratory setting, linear polarization offers researchers the ability to analyze corrosion rates of different alloys as a function of several different factors, including electrolyte selection, dissolved oxygen content, inhibitor selection and concentration, pH and temperature. Because of this, the method has been established as one of the main characterization techniques for corrosion inhibitor systems; indeed, it has become almost expected to encounter LPR analysis when perusing literature dealing with corrosion inhibitors.

In this work, two LPR experimental setups were used in order to evaluate corrosion inhibition efficiency of the candidate molecules under various electrolyte conditions. The first experiment was used to investigate the corrosion rates and inhibition efficiencies of all eight inhibitors, using 3.5% (w/v) NaCl as the electrolyte, with the intent of using these results as the down-selection criteria. Polarization occurred at a rate of 0.1666 mV/s, as suggested by ASTM G59, from -10 mV to + 10 mV vs. E_{corr}.[17] Measurements were made intermittently over a span of 21 days in order to study inhibitor efficiencies as a function of time. The electrochemical cells were stored in a drawer, sealed from the atmosphere with parafilm, only being exposed during the testing. Additionally, because alcohol-amines have been shown to be effective inhibitors of carbon steel, ethanolamine and triethanolamine were also incorporated into this experimental setup as

controls in order to compare results.[6,18–21] Five replicates were performed under each environmental condition.

The second LPR experimental setup examined the use of 1 M HCl as the electrolyte. Various concentrations of the down-selected inhibitors, adrenalone, DOPAC and dopamine, were investigated. A commercial zinc phthalate anticorrosion additive, as well as ethanolamine and triethanolamine, were incorporated into the study for comparison of results. Polarization occurred at a rate of 0.1666 mV/s between -25 mV and +25 mV vs. E_{corr}. Tests began at 0, 1, 3 and 22 hours after solution application. Three replicates were performed for each condition. The potentiostat parameters for each LPR setup are summarized, in Table 2.3.

Table 2.3. Test parameters for linear polarization resistance measurements. Experiments in 3.5% (w/v) NaCl are prior to down-selection of inhibitors, while 1 M HCl experiments are after.

Test Solution	3.5% (w/v) NaCl	1 M HCl
Initial E (V) [vs. E_{corr}]	-0.01	-0.025
Final E (V) [vs. E_{corr}]	0.01	0.025
Scan Rate (mV/s)	0.1666	0.1666
Sample Period (s)	2	2
Sample Area (cm^2)	1	1
Density (g/cm^3)	7.87	7.87
Equivalent Weight	27.92	27.92
Beta An. (V/Decade)	0.12	0.12
Beta Cat. (V/Decade)	0.12	0.12
Initial Delay (s)	1800	1800

2.2.6. Electrochemical Impedance Spectroscopy (EIS)

The electrochemical impedance spectroscopy (EIS) technique is of a different nature than PDS and LPR, both of which operate under direct current (dc) conditions. Instead, EIS evaluates the properties of an electrochemical system as a function of frequency of a small alternating current (ac) signal. Due to the small potential applied in EIS, the test is non-destructive. In general, the

technique reveals different time constants of the system that are relevant to the electrochemical kinetics of the processes occurring on the electrode surface. These processes absorb electrical energy at certain frequencies, creating a time lag between the excitation and response signals; the excitation signal is the applied sinusoidal potential, *V(t)*, whereas the response is the time-dependent measured current *I(t)*. The two terms are related through the following relationship:

$$Z(\omega) = \frac{V(t)}{I(t)} \qquad \text{(Eq. 17)}$$

where *Z(ω)* is the impedance, dependent upon the angular frequency, *ω*, described by ac excitation signal and the time-dependent current response interaction. Eq. 17 is analogous to Ohm's Law, which is applicable under direct current situations, instead of resistance, though, impedance (*Z(ω)*) is inserted in its place for application to time-dependent alternating current applications. Thus, similar to resistance, the impedance is a measure of a system's opposition to electron flow – increased impedance in ac applications is analogous to increased resistance. The time lag of the current in response to the applied ac signal is measured by the phase angle, *θ*.[2] An in-phase (0˚) response is associated with resistive effects, while an out-of-phase (90˚) response is capacitive in nature; the phase angle behavior of the system correlates to the physical processes occurring on the electrode and in solution.

Just like in LPR, polarization resistance (R_p) can be determined with impedance spectroscopy, but requires the aid of circuit modeling software that can fit the spectra with various combinations of circuit elements, assigning values to each. Circuit modeling software is used to obtain a mechanistic idea of the electrochemical processes within the system – for example, R_s in each model of Figure 2.3 is included to account for the resistive solution behavior, whereas C_{dl} represents the capacitive-like behavior of a coating or adsorbed layer of inhibitor molecules. Being

able to measure polarization resistance with EIS gives researchers another method to evaluate and/or confirm corrosion inhibitor performance.[22]

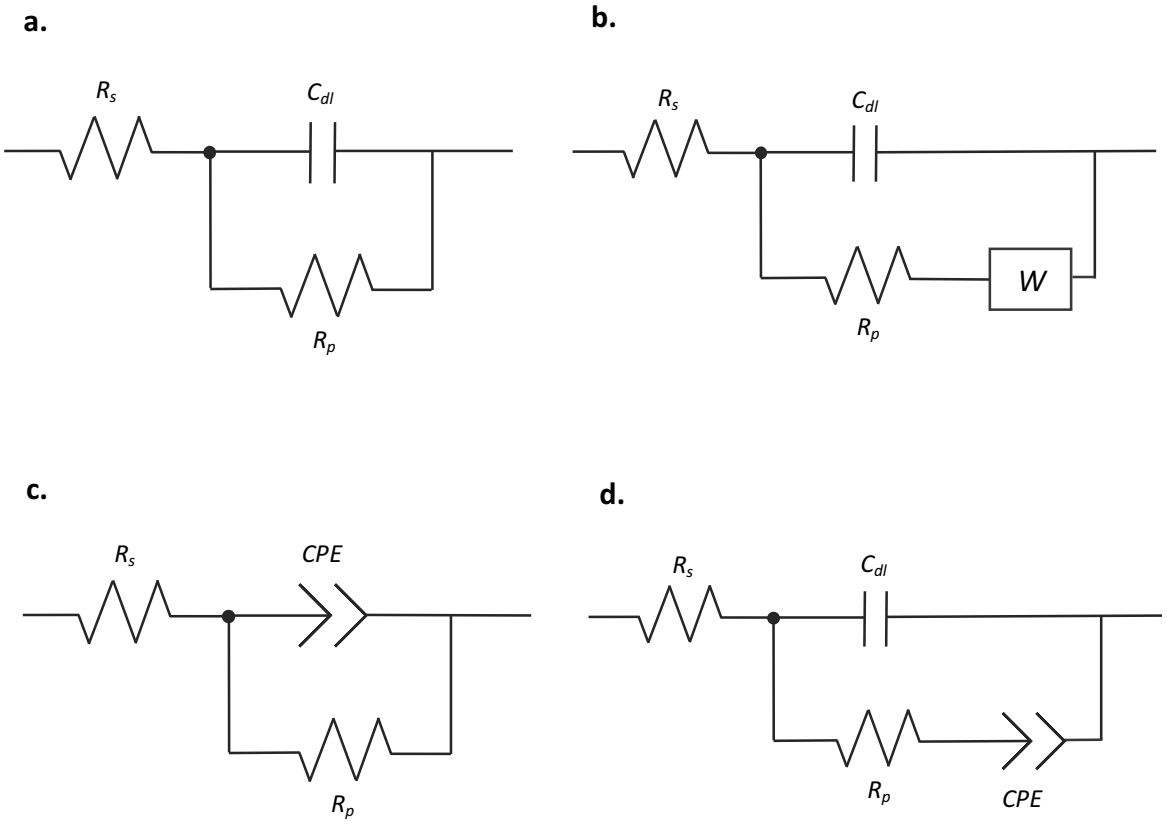

Figure 2.3. Various EIS circuit models used to fit impedance spectra.

In this work, EIS was performed on the down-selected inhibitors under both 3.5% NaCl (w/v) and 1 M HCl conditions. The perturbation signal was applied at 10 mV rms about the corrosion potential. Five data points per decade were collected over a frequency from 100,000 to 0.01 Hz. Three replicates were performed for each condition. The potentiostat parameters for EIS testing are summarized in Table 2.4.

Table 2.4. Test parameters for electrochemical impedance spectroscopy with down-selected inhibitors.

Test Solution	3.5% NaCl	1 M HCl
DC Voltage (V)	0	0
AC voltage (mV rms)	10	10
Initial Frequency (Hz)	100000	100000
Final Frequency (Hz)	0.01	0.01
Points/decade	5	5
Area (cm^2)	1	1
Initial Delay (s)	600	1800

2.3. Results and Discussion

2.3.1. Open Circuit Potential (OCP)

The shift in corrosion potential of mild steel under the influence of organic inhibitor molecules was investigated using OCP monitoring over a period of 18 hours. Four inhibitor systems, including 4-aminosalicylic acid, 5-aminosalicylic acid, allantoin and betaine, show little effect on the corrosion potential, as seen in Figure 2.3. Each system resulted in potentials within about 20 mV of the blank control, a minor shift that is near the allowable variation typically observed for reference electrode measurements, ± 10 mV. Potential shifts within this range are insignificant, and shifts just slightly outside this range indicate minimal effects on the electrochemical system.

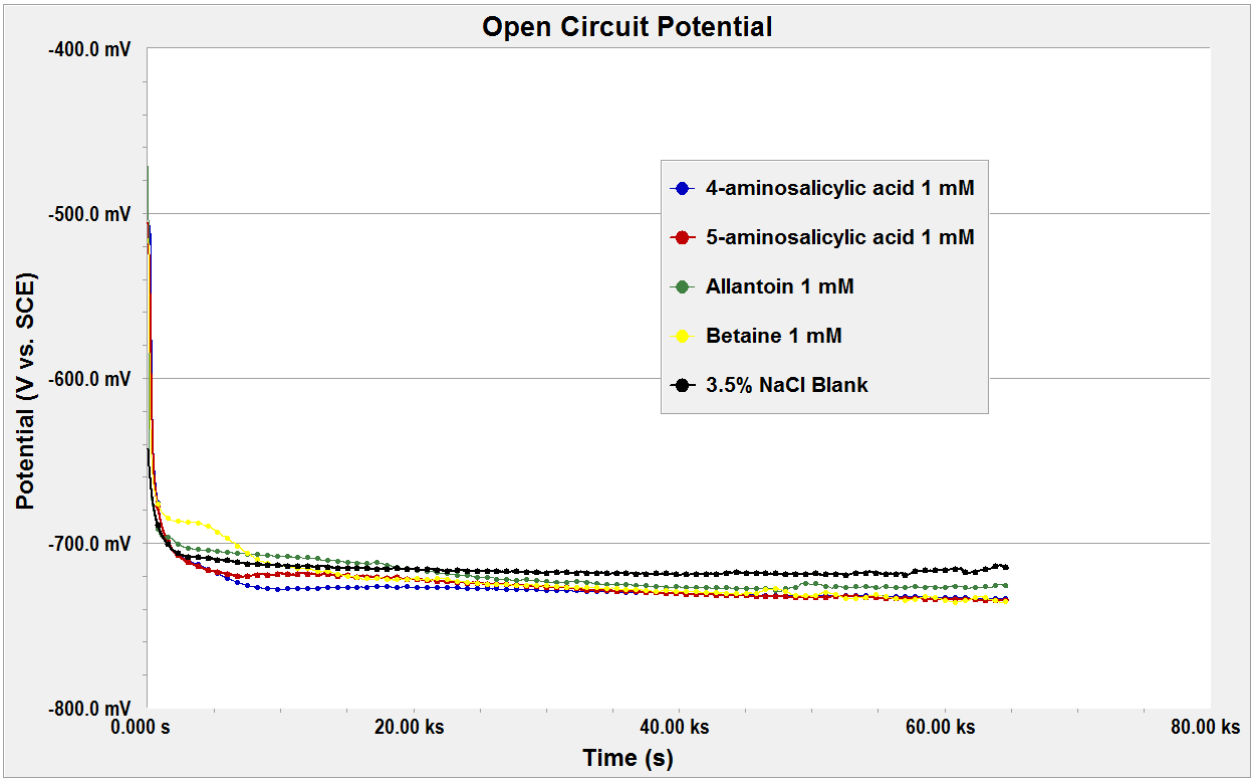

Figure 2.4. Open circuit potential of inhibitors that show minimal shift in E_{corr}.

The other four inhibitors, adrenalone, diazolidinyl urea, DOPAC and dopamine, show much larger shifts in the corrosion potential (Figure 2.4). Each system resulted in shifts above 30 mV, all in the positive direction, with several reaching far beyond this value. It has been proposed that a positive shift in potential is due to the adsorption of inhibitor molecules to the substrate, blocking the anodic and cathodic reaction sites and lowering the corrosion rate.[23–25] Inhibitor concentration is a good indicator of potential shift, with higher concentrations resulting in greater potential difference. The 10 mM DOPAC system resulted in the greatest change in corrosion potential (+128 mV); adrenalone followed, reaching a +78 mV shift at 1 mM concentration. Dopamine required a sufficiently large concentration in order to actually show significant effects, a 50 mM concentration pushed E_{corr} from -717 mV to -678 mV, a shift of +39 mV.

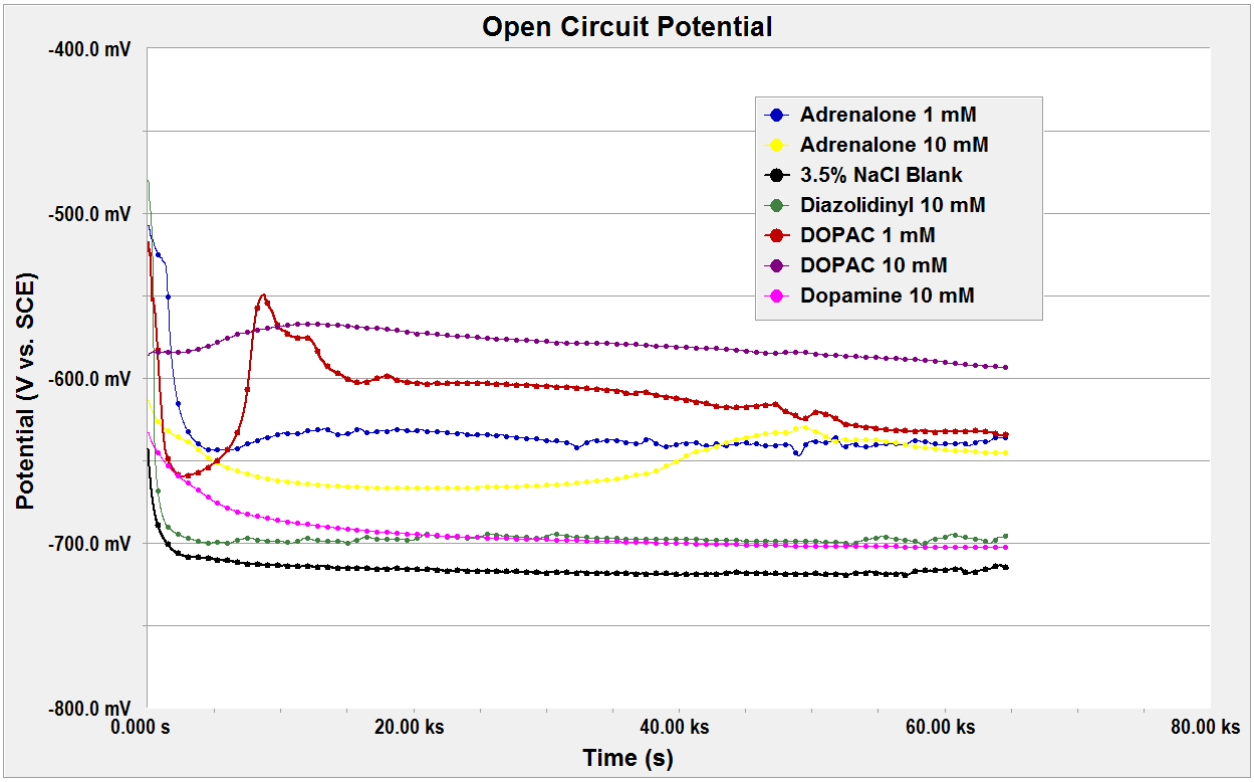

Figure 2.5. Open circuit potential of inhibitors that show a significant shift in E_{corr}.

The idea behind performing this experiment is that organic molecules that display larger shifts in corrosion potential are correlated to having greater substrate interaction, so screening inhibitor molecules with this experiment can give an early indication if future, more revealing tests, would be necessary. Full results for each inhibitor system are displayed in Table 2.5.

Table 2.5. Open circuit potential for inhibitor systems and resultant corrosion potential shift from the control.

Inhibitor	Concentration (M)	Stabilized OCP (V)	Shift (mV)
Control	-	-0.717	-
4-aminosalicylic acid	1.00E-04	-0.731	-14
	1.00E-03	-0.730	-13
	1.00E-02	-0.734	-17
5-aminosalicylic acid	1.00E-04	-0.737	-20
	1.00E-03	-0.732	-15
	1.00E-02	-0.737	-20
Adrenalone HCl	1.00E-04	-0.711	6
	1.00E-03	-0.639	78
	1.00E-02	-0.664	53
Allantoin	1.00E-04	-0.729	-12
	1.00E-03	-0.724	-7
	1.00E-02	-0.727	-10
Betaine	1.00E-04	-0.739	-22
	1.00E-03	-0.729	-12
	1.00E-02	-0.735	-18
Diazolidinyl Urea	1.00E-04	-0.698	19
	1.00E-03	-0.708	9
	1.00E-02	-0.683	34
DOPAC	1.00E-04	-0.736	-19
	1.00E-03	-0.633	84
	1.00E-02	-0.589	128
Dopamine	1.00E-04	-0.703	14
	1.00E-03	-0.700	17
	1.00E-02	-0.678	39

2.3.2. Potentiodynamic Scanning (PDS)

PDS was carried out in order to obtain Tafel constants, β_a and β_c, that are critical descriptors for the polarization curve immediately surrounding the corrosion potential. The Tafel constants are used to identify the slope of the linear behavior displayed. β_a and β_c are used in LPR analysis

to calculate the corrosion rates of metal substrates, which is the rationale for including this technique into the electrochemical characterization model.

Tafel constants for each inhibitor system were extracted from individual anodic and cathodic polarization scans using a least squares fitting technique incorporated into analysis software supplied by Gamry. Figure 2.6 shows an example of the fitting procedure utilized for the 10 mM DOPAC system.

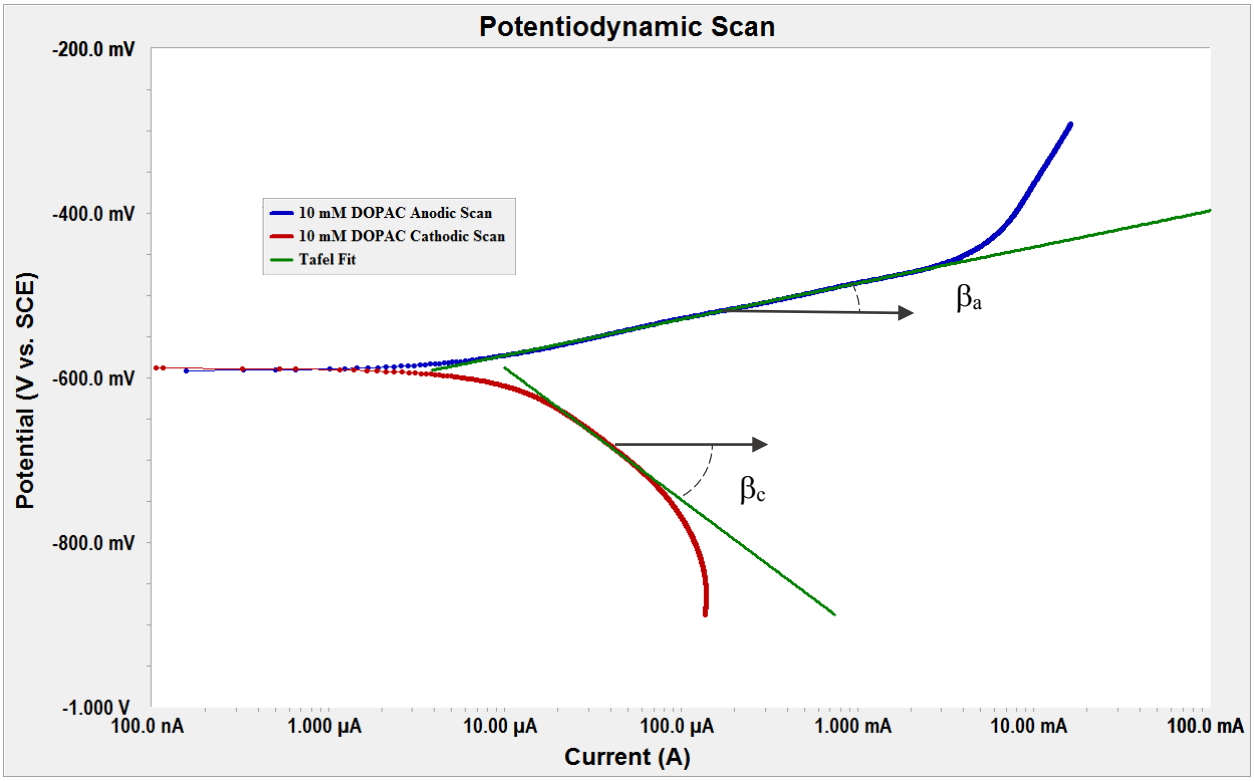

Figure 2.6. Polarization curves of 10 mM DOPAC showing Tafel fitting.

Because separate anodic and cathodic scans were performed, the software required user input to select the region in which to apply the fitting technique. This undoubtedly incorporates some subjectivity in selecting the ideal portion of the curve that models the linear behavior, however literature has indicated Tafel regions in many polarization curves to be somewhat ambiguous, sometimes devoid of explicit linear behavior.[2] This is the case with the cathodic curve

seen in Figure 2.6; although a linear region is present, it is not as distinct as the anodic curve. In literature, this behavior has been attributed to the complex behavior of several cathodic reactions occurring at the surface, simultaneously.[14,26,27]

The results of the Tafel fit procedure for each inhibitor system in 3.5% (w/v) NaCl electrolyte are displayed in Table 2.6. It should be noted that the expected range for β_a, under 3.5% (w/v) NaCl electrolyte conditions, is from about 60 mV to 120 mV, and $\geq$ 60 mV for β_c, but slight variation is not uncommon, especially for cathodic Tafel values.[28] The β_a values obtained from these experiments fall on the lower end of the range, and show little variation across all inhibitor systems, suggesting that these inhibitors have little impact on the slope of the polarization curves when compared to the control solution. The cathodic Tafel constants show similar behavior, also falling on the lower end of the expected range with little variation. It is worth mentioning that, as described by Eq.16, i_{corr} is not very sensitive to the Tafel constants, with both β_a and β_c terms found in the numerator and denominator.[2,27,29] Overall, these results suggest that the practice of estimating β_a and β_c values based on known electrode and solution compositions is acceptable, however determining values individually for each system will yield the most accurate results.

Table 2.6. Anodic and cathodic Tafel constants determined from PDS scans performed in 3.5% NaCl electrolyte.

Inhibitor	Concentration (M)	β_a (mV/decade)	β_c (mV/decade)
Blank	-	59	63
4-aminosalicylic acid	1.00E-05	58	66
	1.00E-04	54	59
	1.00E-03	56	67
5-aminosalicylic acid	1.00E-05	54	73
	1.00E-04	54	63
	1.00E-03	54	68
Adrenalone HCl	1.00E-04	57	68
	1.00E-03	50	62
	1.00E-01	56	62
Allantoin	1.00E-04	57	73
	1.00E-03	56	75
	1.00E-01	49	68
Betaine	1.00E-04	54	70
	1.00E-03	57	68
	1.00E-01	56	58
Diazolidinyl Urea	1.00E-04	53	65
	1.00E-03	51	60
	1.00E-01	53	62
DOPAC	1.00E-04	58	71
	1.00E-03	69	69
	1.00E-01	45	60
Dopamine	1.00E-04	54	70
	1.00E-03	58	66
	1.00E-01	58	66
Ethanolamine	1.00E-04	70	76
	1.00E-03	54	63
	1.00E-02	72	67
Triethanolamine	1.00E-04	59	75
	1.00E-03	58	67
	1.00E-02	70	62

In addition to the Tafel constant determination, PDS scans were performed in order to qualitatively evaluate the passivity behavior of mild steel exposed to the down-selected organic

inhibitors. Mild steel displays passivation behavior under significantly oxidizing conditions, such as exposure to concentrated nitric acid, however 3.5% (w/v) NaCl and 1 M HCl environments only result in slight passivation behavior, with small reductions in current observed.[2,14] Figure 2.7 displays polarization scans over an 8 V range in 3.5% NaCl (w/v) electrolyte for 1 mM concentrations of the down-selected inhibitors. Ethanolamine and triethanolamine at 1 mM concentration are also shown for comparison. The slight depression in corrosion current seen from about 1 V to 3 V is the passivation range. DOPAC shows the lowest passive current of all tested solutions, but only by a slim margin.

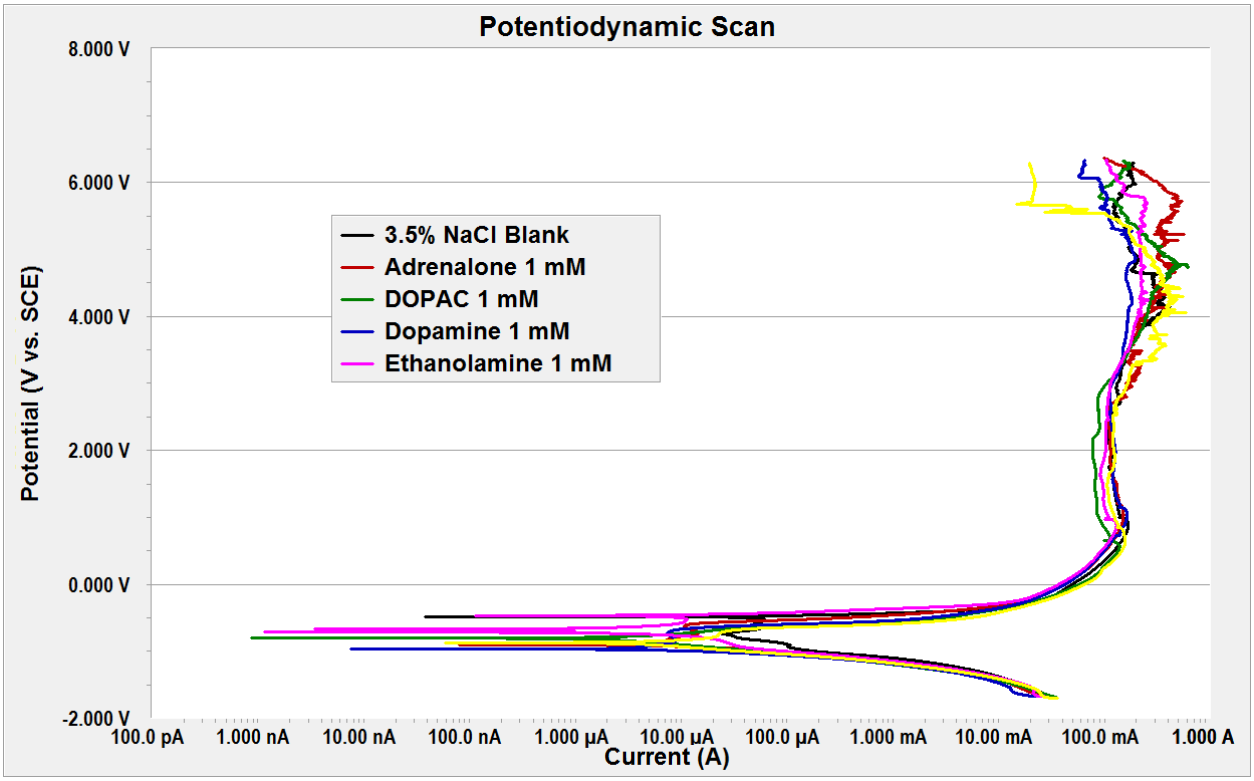

Figure 2.7. PDS scans of down-selected inhibitors in 3.5% NaCl.

Perhaps the more interesting aspect of the polarization curves in Figure 2.7 occurs around E_{corr}, where the control solution appears to display slightly higher currents, especially leading into

the cathodic branch. This trend suggests that the inhibited solutions offer slightly improved corrosion control in the NaCl electrolyte, specifically by suppressing the cathodic current.

Figure 2.8 displays the polarization scans in 1 M HCl electrolyte. Passivation behavior is more accentuated with the acidic electrolyte, showing depressed currents from about 1 V to 3 V. The commercial zinc phthalate inhibitor appears to actually remove any passivation effects that would otherwise be present in the blank solution. Also notice that passivity of the surface with ethanolamine and triethanolamine is not attained until well after 1 V, with currents in the passivation range measuring greater than the control. On the other hand, adrenalone and DOPAC solutions promote passivation prior to reaching 1 V along the polarization curve, with DOPAC displaying the lowest passivation current measured. Better corrosion inhibition performance would be expected for adrenalone and DOPAC in comparison to ethanolamine and triethanolamine; these inhibitor solutions promote passivation sooner (and at lower currents), reducing the time spent in the active state and lowering the overall corrosion of the system.

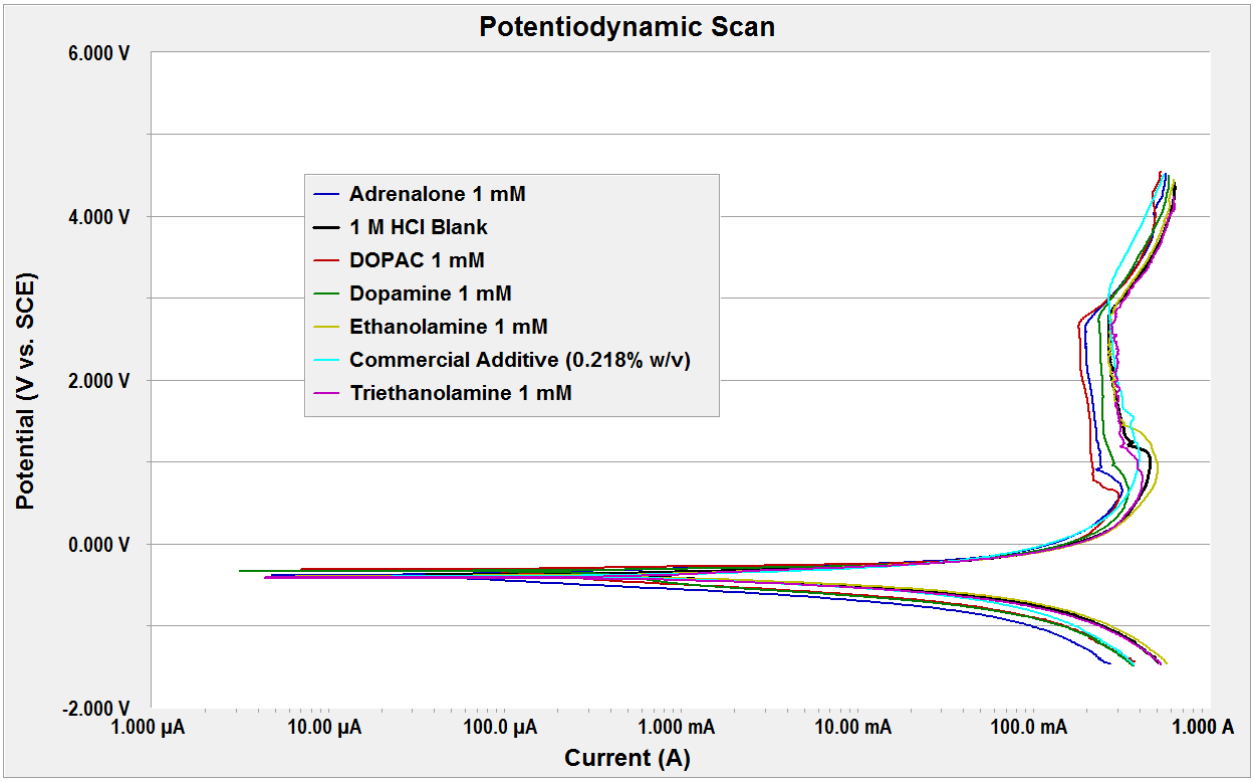

Figure 2.8. PDS scans of down-selected inhibitors in 1 M HCl.

On the cathodic branch of the polarization curve, both ethanolamine and triethanolamine show slightly higher cathodic currents in comparison to the control, whereas adrenalone and DOPAC are slightly lower. These polarization behaviors suggest poor corrosion inhibition for the alkanolamine substances, and improved corrosion resistance for adrenalone and DOPAC. Dopamine tends to follow the same trend as the uninhibited solution, suggesting a higher concentration might be necessary to observe inhibition effects for this molecule.

Another point worth noting is the overall shift in polarization curves under the two electrolyte conditions. Comparing the resultant currents in Figures 2.7 and 2.8 shows a fairly large discrepancy, especially considering the logarithmic scale. To better visualize the difference, 1 mM DOPAC test results under both conditions is displayed in Figure 2.9. It is easy to see the clear increase in corrosion current under acidic conditions, with some portions of the curve displaying

a difference of over two orders of magnitude. This can be attributed to the highly corrosive nature of hydrochloric acid in comparison to the 3.5% NaCl electrolyte – acid solutions provide large amounts of H^+ that fuel the hydrogen evolution reaction and thus, drive the overall corrosion of the system.

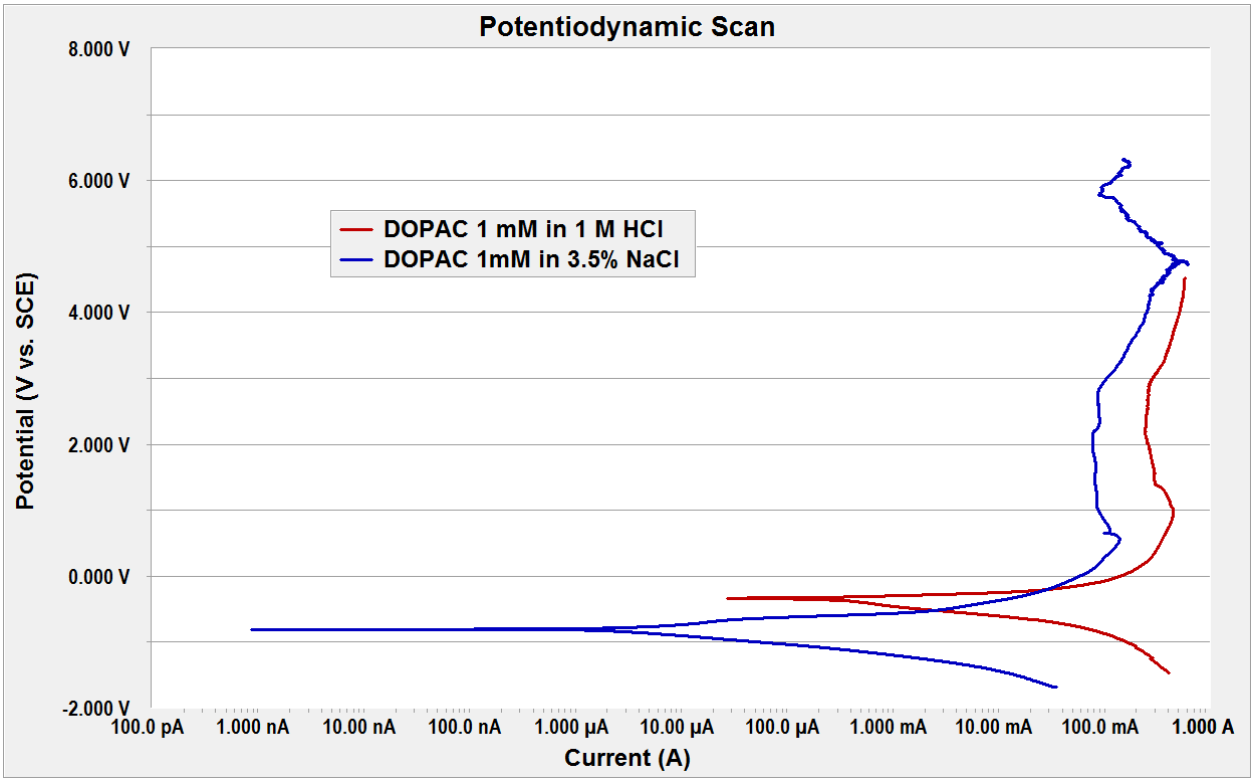

Figure 2.9. Comparison of PDS scans of 1 mM DOPAC exposed to 3.5% NaCl and 1 M HCl.

2.3.3. Linear Polarization Resistance (LPR)

Calculation of corrosion rates, which were used to evaluate the efficiency of the corrosion inhibitors, was facilitated by use of linear polarization resistance. LPR was used to determine polarization resistance, R_p, which in turn was inserted into Eq. 16, along with previously determined Tafel constants (β_a and β_c), in order to calculate the corrosion current density, i_{corr}. Corrosion current density is a measure of how many electrons pass across the substrate within a given area during corrosion processes. Because it is reasonable to assume the entirety of the electric

current originates from the oxidation of carbon steel, i_{corr} is directly proportional to the amount of metal dissolution, as shown by the following modified version of Faraday's law:

$$\mathrm{CR} = \frac{i_{corr} \cdot K \cdot EW}{d} \qquad \text{(Eq. 18)}$$

where CR is the corrosion rate, EW is the equivalent weight of the carbon steel alloy, d is the density of the alloy and K is a proportionality constant used to define the units for the corrosion rate.[30] In this work, corrosion rates are expressed in mils per year (mpy).

Corrosion rates were determined for each of the initial eight inhibitors at various concentrations in 3.5% (w/v) NaCl in order to rank their corrosion inhibition efficiency (%IE), calculated using Eq. 12. Down-selection of the inhibitors was primarily influenced by these results, with those displaying good corrosion inhibition performance sustained over the course of the 21-day incubation period warranting further investigation, including additional LPR analysis in 1 M HCl electrolyte, as well as XPS and QCM surface characterization.

Generally, 4-aminosalicylic acid, 5-aminosalicylic acid, adrenalone, allantoin, diazolidinyl urea, DOPAC and dopamine each displayed lower corrosion rates at higher concentrations over the entire 21-day period. Adrenalone, DOPAC and dopamine each sustained inhibition efficiencies around 50% for the test period, reaching maximums of 58.3% for adrenalone, 58.2% for DOPAC and 66.8% for dopamine. Diazolidinyl urea followed close behind, reaching a maximum of 43.1% inhibition efficiency.

There were, however, several exceptions to the general trend mentioned above. Upon initial tests at Day 0, 4-aminosalicylic, 5-aminosalicylic and allantoin displayed little to no inhibition whatsoever. Instead, 4-aminosalicylic acid and 5-aminosalicylic acid actually caused slightly higher rates of corrosion in comparison to the control sample. Their performance improved significantly over time though, reaching maximum inhibition efficiencies of 43.3% and 38.9% at

1 mM concentration on Day 14 for 4-aminosalicylic acid and 5-aminosalicylic acid, respectively. Allantoin peaked at 60.0% inhibition efficiency at 10 mM concentration on Day 7, but generally achieved only moderate corrosion inhibition performance otherwise, especially at 0.1 mM and 1 mM concentrations.

After Day 0 testing, betaine actually displayed higher corrosion rates with increasing inhibitor concentration. Betaine reached a maximum inhibition efficiency of 51.6% on Day 21 at 0.1 mM, but otherwise was consistently providing only slight corrosion inhibition, and in some cases, was causing higher corrosion rates. This behavior is difficult to account for; however, it is possible that instead of immediately adsorbing directly to the carbon steel surface, small amounts of betaine may instead interact synergistically with iron oxide corrosion product over time, forming a better protective oxide layer than would otherwise be expected. Further inspection of this behavior is recommended for future studies.

Additionally, ethanolamine and triethanolamine were included in this study for comparison, as alcohol amines have been shown to be effective corrosion inhibitors for steel rebar in alkaline environments.[6,18,31–33] Under these conditions, ethanolamine displayed relatively poor inhibition, generally showing diminished performance at higher concentrations, reaching peak efficiency on Day 21 of only 36.5%. Triethanolamine results show some corrosion inhibition upon initial application at Day 0 (25.7%), but performance quickly deteriorates over time and ultimately displays the worst performance of all inhibitors examined. Testing in a more acidic environment inundated with Cl^- may have impeded the performance typically seen of alcohol amines, as similar findings have been observed with dimethylethanolamine (DMEA).[18] Furthermore, steric effects of the branched triethanolamine molecule may have prevented tight surface packing during

adsorption on the carbon steel, resulting in small gaps in surface coverage that provide less protection against corrosion.

Greater inhibitor concentrations yielding better inhibition performance is a distinctive feature of organic inhibitors that function through an adsorptive mechanism. As largely observed in these results, every inhibitor (except betaine) followed this trend, suggesting they function as classic organic inhibitors. As more inhibitor is added to the system, increased surface coverage occurs, leading to a more uniform protective layer on the surface.

Based on these initial linear polarization results, it was decided that sustained inhibition efficiencies of 50% or more over the course of the testing period would be the down-selection criterion. This led to continued investigation of adrenalone, DOPAC and dopamine, while the other chemicals ceased their progress through the inhibitor characterization test method. LPR results in 3.5% (w/v) NaCl electrolyte from 0 to 21 days are displayed in Tables 2.7 - 2.10, respectively.

Table 2.7. Electrochemical parameters determined from LPR measurements in 3.5% NaCl in the presence and absence of various inhibitor concentrations at 0 days incubation.

Inhibitor	Concentration	E_{corr}	I_{corr}	R_p	Corr. Rate	Efficiency
	(M)	(mV)	($\mu A \cdot cm^{-2}$)	(Ω)	(mpy)	(%)
Blank	-	-724.87	17.17	1576	7.85	-
4-aminosalicylic acid	1.00E-04	-681.98	31.86	827	14.56	-85.56
	1.00E-03	-696.26	18.33	1422	8.37	-6.72
5-aminosalicylic acid	1.00E-04	-703.40	17.69	1472	8.09	-3.06
	1.00E-03	-688.96	20.70	1259	9.46	-20.57
Adrenalone HCl	1.00E-04	-678.58	18.10	1445	8.27	-5.43
	1.00E-03	-652.94	13.71	1909	6.26	20.16
	1.00E-02	-598.66	8.84	2950	4.04	48.52
Allantoin	1.00E-04	-728.14	15.86	1657	7.25	7.62
	1.00E-03	-734.48	19.65	1326	8.98	-14.43
	1.00E-02	-725.48	18.50	1409	8.46	-7.76
Betaine	1.00E-04	-715.46	16.88	1546	7.71	1.70
	1.00E-03	-725.60	12.66	2069	5.79	26.25
	1.00E-02	-698.64	14.82	1760	6.77	13.67
Diazolidinyl Urea	1.00E-04	-690.62	16.24	1610	7.42	5.42
	1.00E-03	-699.30	11.50	2285	5.25	33.03
	1.00E-02	-693.00	10.37	2521	4.74	39.60
DOPAC	1.00E-04	-685.14	15.39	1696	7.03	10.38
	1.00E-03	-689.12	17.73	1476	8.10	-3.27
	1.00E-02	-573.70	11.27	2314	5.15	34.38
Dopamine	1.00E-04	-657.72	13.08	1995	5.98	23.82
	1.00E-03	-672.74	14.07	1851	6.43	18.03
	1.00E-02	-650.58	10.58	2462	4.84	38.35
Ethanolamine	1.00E-04	-718.16	14.66	1778	6.70	14.62
	1.00E-03	-728.50	11.48	2276	5.25	33.15
	1.00E-02	-613.46	11.35	2363	5.19	33.91
Triethanolamine	1.00E-04	-719.64	13.67	1910	6.25	20.38
	1.00E-03	-711.42	14.94	1745	6.83	12.99
	1.00E-02	-678.64	12.76	2045	5.83	25.69

Table 2.8. Electrochemical parameters determined from LPR measurements in 3.5% NaCl in the presence and absence of various inhibitor concentrations after 7 days of incubation.

Inhibitor	Concentration (M)	E_{corr} (mV)	I_{corr} ($\mu A \cdot cm^{-2}$)	R_p (Ω)	Corr. Rate (mpy)	Efficiency (%)
Blank	-	-728.79	14.56	1790	6.65	-
4-aminosalicylic acid	1.00E-04	-728.32	12.42	2097	5.68	14.68
	1.00E-03	-744.70	9.26	2813	4.23	36.40
5-aminosalicylic acid	1.00E-04	-734.04	13.91	1873	6.36	4.47
	1.00E-03	-738.92	10.73	2429	5.10	23.32
Adrenalone HCl	1.00E-04	-745.42	12.20	2136	5.58	16.21
	1.00E-03	-664.84	8.81	2967	4.03	39.49
	1.00E-02	-583.30	8.06	3308	3.68	44.68
Allantoin	1.00E-04	-731.12	16.41	1601	7.50	-12.71
	1.00E-03	-727.92	13.92	1878	6.36	4.42
	1.00E-02	-726.78	5.83	4473	2.66	59.98
Betaine	1.00E-04	-747.40	13.36	1960	6.11	8.23
	1.00E-03	-747.74	13.67	1912	6.25	6.15
	1.00E-02	-735.66	14.95	1746	6.83	-2.66
Diazolidinyl Urea	1.00E-04	-709.52	13.67	1910	6.24	6.15
	1.00E-03	-685.82	12.16	2177	5.55	16.52
	1.00E-02	-696.52	10.48	2502	4.79	28.06
DOPAC	1.00E-04	-739.06	10.23	2549	4.67	29.75
	1.00E-03	-675.48	8.41	3100	3.83	42.51
	1.00E-02	-600.38	7.45	3502	3.40	48.87
Dopamine	1.00E-04	-732.54	13.75	1897	6.28	5.58
	1.00E-03	-646.02	12.17	2144	5.56	16.41
	1.00E-02	-664.18	4.83	5396	2.21	66.84
Ethanolamine	1.00E-04	-740.82	11.41	2284	5.21	21.67
	1.00E-03	-736.20	13.10	1989	5.99	10.04
	1.00E-02	-584.42	15.76	1654	7.20	-8.20
Triethanolamine	1.00E-04	-746.80	15.26	1707	6.97	-4.80
	1.00E-03	-747.14	16.44	1585	7.51	-12.91
	1.00E-02	-606.66	18.00	1448	8.22	-23.59

Table 2.9. Electrochemical parameters determined from LPR measurements in 3.5% NaCl in the presence and absence of various inhibitor concentrations after 14 days of incubation.

Inhibitor	Concentration (M)	E_{corr} (mV)	I_{corr} ($\mu A \cdot cm^{-2}$)	R_p (Ω)	Corr. Rate (mpy)	Efficiency (%)
Blank	-	-728.74	18.13	1445	8.28	-
4-aminosalicylic acid	1.00E-04	-747.12	9.31	2303	5.17	37.61
	1.00E-03	-748.02	10.29	2533	4.70	43.28
5-aminosalicylic acid	1.00E-04	-719.54	20.53	1269	9.38	-13.25
	1.00E-03	-741.34	11.99	2174	5.48	33.89
Adrenalone HCl	1.00E-04	-732.68	21.57	1208	9.86	-18.97
	1.00E-03	-663.54	12.16	2145	5.56	32.92
	1.00E-02	-590.12	7.56	3446	3.46	58.29
Allantoin	1.00E-04	-724.02	17.80	1468	8.13	1.85
	1.00E-03	-754.72	15.83	1647	7.23	12.71
	1.00E-02	-743.00	11.87	2201	5.42	34.56
Betaine	1.00E-04	-732.52	10.58	2074	5.75	30.63
	1.00E-03	-741.76	11.54	2265	5.27	36.37
	1.00E-02	-734.40	19.77	1318	8.95	-8.09
Diazolidinyl Urea	1.00E-04	-709.70	13.48	1934	6.16	25.67
	1.00E-03	-720.42	10.63	2481	4.86	41.39
	1.00E-02	-693.86	11.76	2276	5.37	35.13
DOPAC	1.00E-04	-744.54	14.04	1856	6.41	22.58
	1.00E-03	-654.18	7.58	3457	3.46	58.18
	1.00E-02	-615.80	8.56	3045	3.91	52.77
Dopamine	1.00E-04	-742.06	17.28	1508	7.89	4.71
	1.00E-03	-697.12	8.82	2960	4.03	51.35
	1.00E-02	-658.52	7.68	3392	3.51	57.64
Ethanolamine	1.00E-04	-731.84	12.78	2039	5.84	29.56
	1.00E-03	-754.78	18.40	1416	8.41	-1.50
	1.00E-02	-585.46	26.05	1003	11.90	-43.66
Triethanolamine	1.00E-04	-728.56	22.74	1151	10.39	-25.47
	1.00E-03	-737.72	26.76	974	10.23	-23.46
	1.00E-02	-646.06	17.01	1532	7.77	6.17

Table 2.10. Electrochemical parameters determined from LPR measurements in 3.5% NaCl in the presence and absence of various inhibitor concentrations after 21 days of incubation.

Inhibitor	Concentration (M)	E_{corr} (mV)	I_{corr} ($\mu A \cdot cm^{-2}$)	R_p (Ω)	Corr. Rate (mpy)	Efficiency (%)
Blank	-	-733.81	15.04	1748	6.87	-
4-aminosalicylic acid	1.00E-04	-751.20	8.62	3023	3.94	42.70
	1.00E-03	-738.14	9.28	2808	4.24	38.32
5-aminosalicylic acid	1.00E-04	-725.40	21.05	1239	9.62	-39.94
	1.00E-03	-748.58	10.54	2473	4.81	29.96
Adrenalone HCl	1.00E-04	-726.00	19.87	1311	9.08	-32.09
	1.00E-03	-665.14	8.34	3123	3.81	44.53
	1.00E-02	-582.88	7.54	3459	3.47	49.50
Allantoin	1.00E-04	-723.90	16.08	1621	7.35	-6.85
	1.00E-03	-726.12	12.65	2059	5.78	15.89
	1.00E-02	-747.20	8.98	2901	4.11	40.29
Betaine	1.00E-04	-748.96	7.02	3710	3.33	51.57
	1.00E-03	-740.00	12.56	2075	5.74	16.50
	1.00E-02	-734.98	16.71	1560	7.64	-11.07
Diazolidinyl Urea	1.00E-04	-730.98	8.60	3032	3.93	42.87
	1.00E-03	-692.88	8.65	3011	3.95	42.48
	1.00E-02	-711.98	8.57	3055	3.92	43.05
DOPAC	1.00E-04	-739.52	12.45	2092	5.69	17.23
	1.00E-03	-695.80	8.46	3082	3.86	43.80
	1.00E-02	-616.52	7.55	3454	3.45	49.83
Dopamine	1.00E-04	-720.92	25.74	1012	11.76	-71.10
	1.00E-03	-692.88	10.10	2582	4.61	32.88
	1.00E-02	-671.74	6.20	4200	2.83	58.76
Ethanolamine	1.00E-04	-738.22	11.81	2206	5.40	21.48
	1.00E-03	-747.28	9.56	2726	4.37	36.47
	1.00E-02	-698.86	12.78	2039	5.84	15.06
Triethanolamine	1.00E-04	-699.86	21.71	1201	9.92	-44.31
	1.00E-03	-744.00	15.54	1677	7.10	-3.28
	1.00E-02	-651.28	17.36	1502	7.93	-15.42

The foundation of this work was to develop a selection process capable of investigating corrosion rates of a larger sampling of molecules in a preliminary testing procedure, before further inhibitor characterization occurs. Linear polarization resistance experiments offer rapid testing and

results that are easy to interpret, making it a convenient electrochemical test for screening a large selection of molecules. This was the premise behind its utilization as the prominent electrochemical test for down-selection, as more importance was placed on the mild steel corrosion rates obtained through LPR than on qualitative PDS investigations. Corrosion rates calculated using Eq. 18 for adrenalone, DOPAC and dopamine inhibitor systems throughout the initial test period are summarized in Figure 2.10. These results depict a general reduction in corrosion rate as inhibitor concentration increases; this trend is especially visible for adrenalone and dopamine. At 10 mM concentrations, corrosion rates for the three down-selected inhibitors were sustained at about 4 mils per years over the 21-day period.

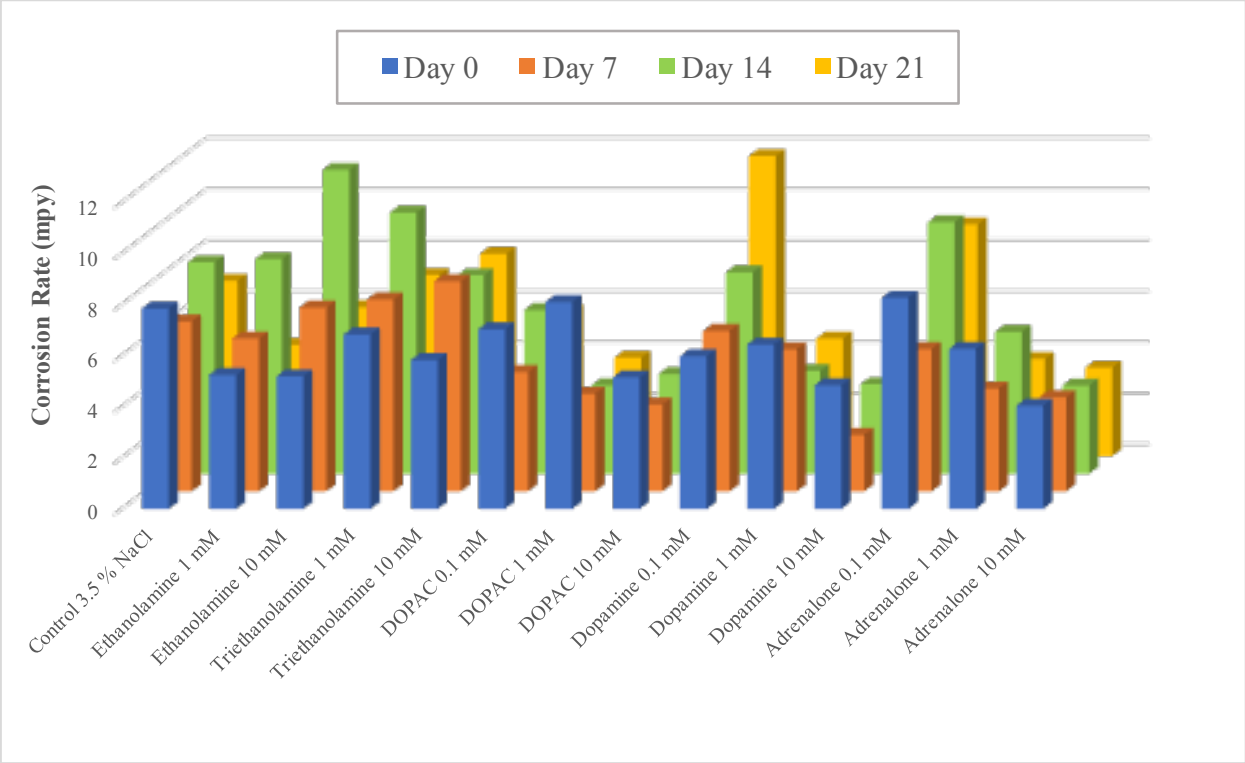

Figure 2.10. Corrosion rates in 3.5% NaCl, calculated using Faraday's Law and polarization resistance (R_p) values determined from LPR.

Further LPR characterization of adrenalone, DOPAC and dopamine in 1 M HCl yielded largely improved inhibition in comparison to the control sample. This time, testing occurred over

a 22-hour period because the acidic media is much more corrosive than the NaCl electrolyte. The organic inhibitors showed excellent inhibitive properties, significantly reducing the corrosion rate at each tested concentration. Corrosion rates were again lower as inhibitor concentration increased. Furthermore, inhibition efficiency improved over time, with each inhibitor system reaching its maximum performance at Hour 22. Ranking the performance of the three down-selected inhibitors at the end of the testing period gives adrenalone > dopamine > DOPAC, with calculated %IE of 95.6%, 90.4% and 85.6%. These values are similar to other studies investigating environmentally-sourced organic inhibitors under similar acidic conditions.[34–42] These authors attributed inhibitor function to adsorption of the molecules to the steel surface, interfering with the corrosion reaction by slowing the process of mass and electron transfer, as suggested in this work. LPR results in 1 M HCl electrolyte from 0 to 22 hours are displayed in Tables 2.11 - 2.14, respectively.

Table 2.11. Electrochemical parameters determined from LPR measurements in 1 M HCl in the presence and absence of various inhibitor concentrations at hour 0.

Inhibitor	Concentration (M)	E_{corr} (mV)	I_{corr} ($\mu A \cdot cm^{-2}$)	R_p (Ω)	Corr. Rate (mpy)	Efficiency (%)
Blank	-	-499.13	306.13	88.86	139.88	-
Adrenalone HCl	1.00E-03	-488.70	91.54	284.70	41.83	70.09
	1.00E-02	-489.83	127.33	212.33	58.17	58.42
DOPAC	1.00E-04	-494.65	151.20	174.30	69.10	50.60
	1.00E-03	-496.33	140.19	193.38	64.08	54.19
	1.00E-02	-489.50	137.20	190.60	62.70	55.18
Dopamine HCl	1.00E-04	-489.00	142.05	183.45	64.90	53.60
	1.00E-03	-493.00	150.63	173.17	68.82	50.80
	1.00E-02	-488.80	125.03	208.87	57.14	59.15
Commercial Additive	0.217 % (w/v)	-487.76	157.40	171.18	71.93	48.57
Ethanolamine	1.00E-03	-494.25	136.30	195.50	62.29	55.47
	1.00E-02	-496.70	208.30	125.55	95.16	31.97
Triethanolamine	1.00E-03	-499.10	208.23	125.20	95.17	31.96
	1.00E-02	-486.23	166.93	159.83	76.28	45.47

Table 2.12. Electrochemical parameters determined from LPR measurements in 1 M HCl in the presence and absence of various inhibitor concentrations at hour 1.

Inhibitor	Concentration (M)	E_{corr} (mV)	I_{corr} ($\mu A \cdot cm^{-2}$)	R_p (Ω)	Corr. Rate (mpy)	Efficiency (%)
Blank	-	-494.50	402.48	70.75	210.50	-
Adrenalone HCl	1.00E-03	-484.60	84.10	312.30	38.46	81.73
	1.00E-02	-486.43	87.24	337.90	39.88	81.06
DOPAC	1.00E-04	-495.60	192.35	138.85	87.90	58.24
	1.00E-03	-494.48	137.22	217.43	62.70	70.21
	1.00E-02	-491.60	124.90	208.55	57.08	72.88
Dopamine HCl	1.00E-04	-490.05	148.05	178.20	67.65	67.86
	1.00E-03	-495.27	174.67	150.40	79.82	62.08
	1.00E-02	-492.87	133.80	195.30	61.13	70.96
Commercial Additive	0.217 % (w/v)	-488.86	164.40	161.50	75.14	64.30
Ethanolamine	1.00E-03	-493.05	128.65	206.55	58.83	72.05
	1.00E-02	-493.50	202.50	131.05	92.52	56.05
Triethanolamine	1.00E-03	-494.17	211.77	123.13	96.76	54.03
	1.00E-02	-487.93	174.43	149.53	79.71	62.13

Table 2.13. Electrochemical parameters determined from LPR measurements in 1 M HCl in the presence and absence of various inhibitor concentrations at hour 3.

Inhibitor	Concentration (M)	E_{corr} (mV)	I_{corr} ($\mu A \cdot cm^{-2}$)	R_p (Ω)	Corr. Rate (mpy)	Efficiency (%)
Blank	-	-487.40	368.63	75.94	199.84	-
Adrenalone HCl	1.00E-03	-477.85	56.27	470.55	25.71	87.13
	1.00E-02	-476.80	45.82	653.73	20.95	89.52
DOPAC	1.00E-04	-479.00	200.25	131.30	91.51	54.21
	1.00E-03	-492.23	125.39	244.43	57.30	71.33
	1.00E-02	-496.70	169.20	154.00	77.32	61.31
Dopamine HCl	1.00E-04	-490.40	193.00	135.00	88.25	55.84
	1.00E-03	-490.70	154.87	171.10	70.77	64.59
	1.00E-02	-489.83	108.80	240.47	49.74	75.11
Commercial Additive	0.217 % (w/v)	-488.30	173.46	119.95	100.93	49.49
Ethanolamine	1.00E-03	-488.80	118.62	237.80	54.25	72.86
	1.00E-02	-489.65	285.20	92.15	130.30	34.80
Triethanolamine	1.00E-03	-488.50	211.60	124.73	96.70	51.61
	1.00E-02	-481.90	216.00	121.40	98.74	50.59

Table 2.14. Electrochemical parameters determined from LPR measurements in 1 M HCl in the presence and absence of various inhibitor concentrations at hour 22.

Inhibitor	Concentration (M)	E_{corr} (mV)	I_{corr} ($\mu A \cdot cm^{-2}$)	R_p (Ω)	Corr. Rate (mpy)	Efficiency (%)
Blank	-	-463.58	744.90	37.84	340.23	-
Adrenalone HCl	1.00E-03	-459.90	32.61	803.20	14.90	95.62
	1.00E-02	-465.07	77.18	404.17	35.27	89.63
DOPAC	1.00E-04	-467.40	195.45	150.73	89.25	73.77
	1.00E-03	-484.35	110.34	257.25	50.42	85.18
	1.00E-02	-482.10	107.45	288.35	49.11	85.57
Dopamine HCl	1.00E-04	-476.00	319.10	82.38	146.05	57.07
	1.00E-03	-485.43	180.70	149.90	82.57	75.73
	1.00E-02	-480.33	71.62	367.77	32.73	90.38
Commercial Additive	0.217 % (w/v)	-474.35	572.85	46.52	261.70	23.08
Ethanolamine	1.00E-03	-469.10	302.10	86.53	138.05	59.42
	1.00E-02	-481.25	855.15	30.65	390.20	-14.69
Triethanolamine	1.00E-03	-475.23	645.27	41.11	295.00	13.29
	1.00E-02	-464.40	569.27	47.07	260.10	23.55

The corrosion rates for inhibitor systems in 1 M HCl are summarized in Figure 2.11. These results highlight the stark contrast in corrosion rates between the control sample and the samples exposed to adrenalone, DOPAC, and dopamine inhibitors, especially as time passed. The reduction in mild steel corrosion afforded by adrenalone, DOPAC and dopamine was slightly better than those of the comparative inhibitors over the first hours of electrolyte exposure. By Hour 22, the comparative inhibitors displayed little reduction in corrosion rates, highlighting the efficiency of the down-selected inhibitors. Apart from 0.1 mM dopamine which displayed a slight increase in corrosion at Hour 22, each inhibitor system sustained low corrosion rates over the duration of testing.

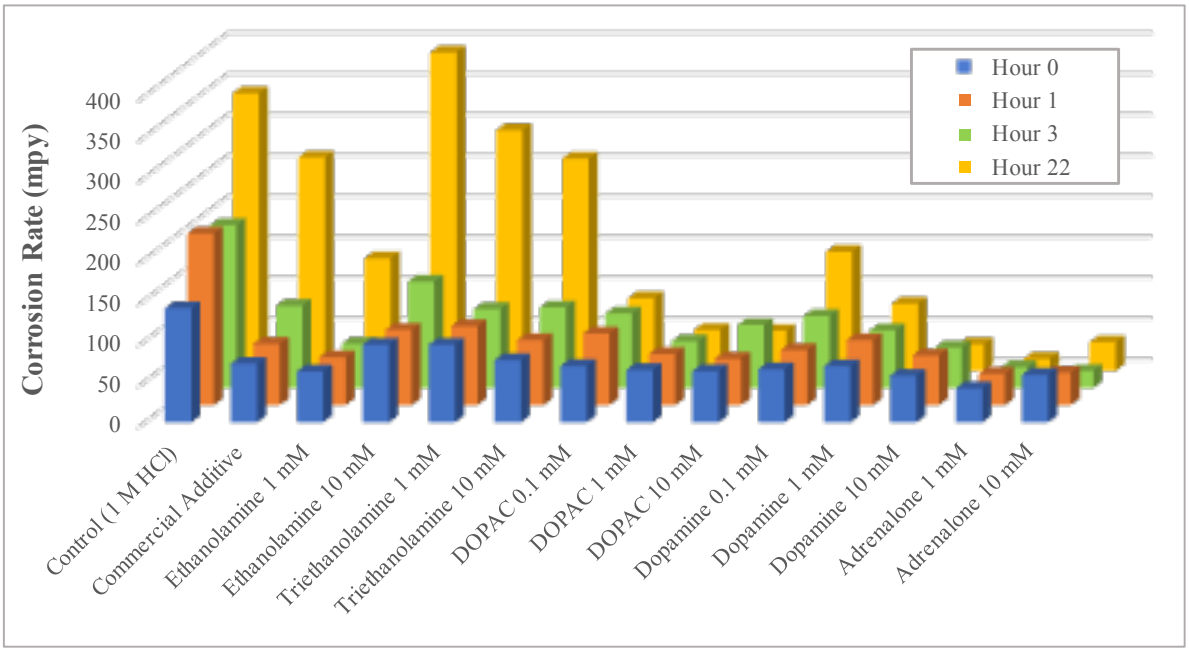

Figure 2.11. Corrosion rates in 1 M HCl, calculated using Faraday's Law and polarization resistance (R_p) values determined from LPR.

The pronounced effect of corrosion inhibition for these molecules applied to acidic conditions, as compared to 3.5% (w/v) NaCl, is considerable. Adrenalone, DOPAC and dopamine each increased inhibition efficiency by more than 30% upon transition to the 1 M HCl solution. This is probably due to the fact that acidic environments are significantly more corrosive to carbon steel, so even slight protection due to the organic inhibitor surface coverage is amplified in comparison to less acidic environments. On the other hand, several authors have presented an adsorption mechanism that is slightly different in acidic environments, incorporating an intermediate step that involves dissolved Cl^- ions.[43–49] Generally, Cl^- promotes corrosion by attack on the passive layer and subsequent breakdown of protective iron oxides, however chloride ions in an acidic environment may actually facilitate initial inhibitor adsorption. Under acidic conditions, the carbon steel surface takes on a positive charge which is specifically adsorbed by the anionic chloride ions. This excess negative charge at the substrate-electrolyte interface leads

to subsequent adsorption of protonated inhibitor molecules through electrostatic interactions. As pointed out by Akrout et al., the interaction between inhibitors, chloride ions and the substrate is difficult to explicitly investigate, however these studies provide at least some insight into the complex interfacial interactions.[50]

The commercial zinc phthalate and alkanolamine inhibitors displayed far less inhibitive properties overall in comparison to the organic inhibitors. As can be seen in Figure 2.10, the zinc phthalate additive performed moderately over the first three hours, reducing the corrosion rate and reaching 64.3% inhibition efficiency. However, by Hour 22, performance dipped to 23.1% efficiency, offering significantly less protection than the organic inhibitors. The zinc phthalate additive is a flash rust inhibitor (a temporary inhibitor that is effective at preventing early forms of corrosion), which might explain why performance deteriorates over time in these conditions. Furthermore, the additive is marketed as being designed for incorporation into waterborne and solvent borne coating systems with other corrosion inhibitor additives,[51] which is not how it was utilized in this study. Ethanolamine and triethanolamine displayed better overall corrosion reduction in hydrochloric acid electrolyte than in 3.5% (w/v) NaCl, consistently performing between 30% and 70% inhibition efficiency for the first three hours of testing. By hour 22 though, corrosion inhibition diminished for the most part. The 1 mM ethanolamine system was the only one that continued to display a good inhibition efficiency (59.4 %) after 22 hours. These results are similar to those obtained by Jeyaprabha et al. investigating alkanolamines in 0.5 M H_2SO_4.[52] The poorer performance of the alkanolamine in comparison to adrenalone, DOPAC and dopamine is most likely a result of being applied in an acidic environment, whereas their usual application is under alkaline environments protecting steel rebar reinforcements in concrete.

2.3.4. Electrochemical Impedance Spectroscopy (EIS)

EIS was performed in order to obtain polarization resistance, R_p, data from inhibited and uninhibited solutions of 1 M HCl, and to obtain mechanistic circuit parameter values for further system characterization. *Echem Analyst* software supplied by Gamry Instruments, Inc. was used to model the impedance spectra obtained. The spectra were fitted to the circuit shown in Figure 2.3 (d), which is the commonly used Randles circuit with an additional constant phase element (CPE) used to fit the data better. CPE is calculated using Eq. 19.

$$\mathrm{CPE} = \mathrm{Y}_o{}^{a} \qquad \text{(Eq. 19)}$$

where Y_o is a variation to capacitance, measured in Farads (F). The Randles circuit contains parameters for modeling solution resistance (R_s), the capacitance of the electric double layer on the metal surface (C_{dl}) and polarization resistance (R_p). Assigned circuit parameter values for each inhibitor system are displayed in Table 2.15.

Table 2.15. Circuit modeling parameters determined from EIS measurements in 1 M HCl in the presence and absence of various inhibitor concentrations.

Inhibitor	Concentration (M)	R_p (Ω)	R_s (Ω)	C_{dl} (F)	Y_o ($S*s^a$)	*a*	Efficiency (%)
Blank	-	0.168	1.611	2.77E-03	4.992	0.322	-
Adrenalone HCl	1.00E-04	0.313	2.386	3.71E-03	6.428	0.258	46.4
	1.00E-03	0.245	1.850	1.98E-03	4.001	0.221	31.7
	1.00E-02	0.220	2.010	2.40E-03	6.198	0.273	23.8
DOPAC	1.00E-04	0.311	2.636	8.10E-04	6.233	0.200	46.1
	1.00E-03	0.294	1.672	8.79E-04	3.159	0.269	43.0
	1.00E-02	0.301	1.840	1.78E-03	6.716	0.245	44.2
Dopamine HCl	1.00E-04	0.321	2.410	2.47E-03	4.013	0.241	47.8
	1.00E-03	0.312	2.218	1.52E-03	4.607	0.312	46.2
	1.00E-02	0.318	1.536	6.43E-05	3.711	0.270	47.3
FR Pigment	0.217 % (w/v)	0.316	2.487	3.40E-02	3.597	0.245	46.9

The inclusion of the CPE is generally an approach used to improve the "goodness of fit", however the circuit parameters that describe the CPE, (Y_o and a) are not extremely telling when trying to relate to the physical processes occurring on the mild steel surface. Instead, the CPE is used to model behavior that lies somewhere between capacitance and resistance. In one study, the mixed behavior modeled with the CPE was associated with surface heterogeneities creating an unevenly distributed current density on the electrode.[53] CPEs have also been used to account for the behavior of non-ideal capacitors as a function of frequency.[22]

The inhibition efficiencies in Table 2.15 were calculated using the modeled polarization resistance parameters for each inhibitor system. It is clear that these values are smaller than those determined through LPR, ranging from about 25% to 50%. These values still indicate corrosion protection is afforded by the inhibitors, however not quite as much as suggested by LPR experiments. Furthermore, the polarization resistance measured through EIS is about 1-2 orders of magnitude smaller than expected. A Nyquist plot of Adrenalone 0.1 mM and 10 mM solutions compared against the control solution is shown in Figure 2.12. Polarization resistance is represented visually as the diameter length across each semi-circle plot. It can be seen that R_p does increase upon addition of inhibitor, but only slightly.

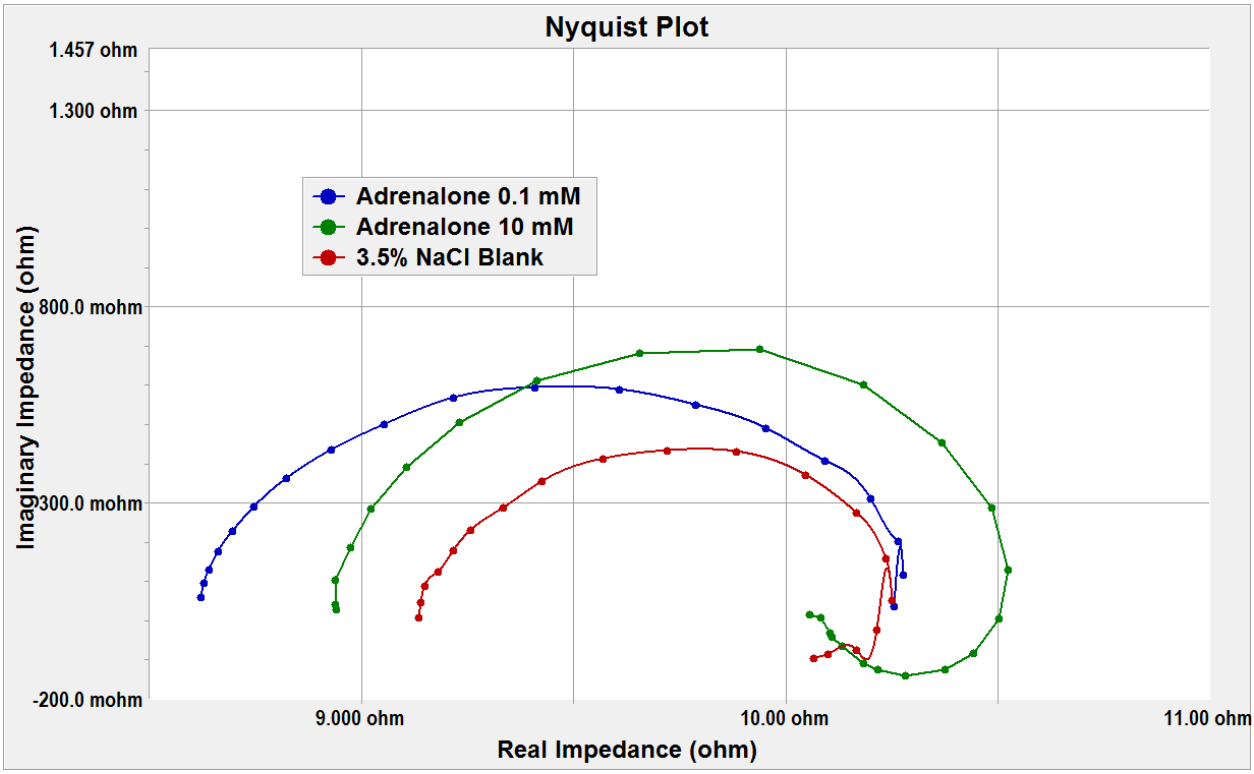

Figure 2.12. Nyquist impedance plot of adrenalone 0.1 mM and 10 mM plotted against 3.5% (w/v) NaCl control.

The low resistance determined through circuit modeling might be a result of incomplete surface coverage of the organic molecules on the substrate surface. This can be related to a similar situation encountered when performing EIS experiments on coated substrates - measured impedance is significantly lower on a coating with a defect than on a perfect coating, indicating loss of barrier properties and reduced corrosion protection. For solutions with organic inhibitors that function through surface adsorption, this situation would result in the impedance of the bare substrate being measured, rather than the covered portions of the surface. Higher concentrations of inhibitor might resolve this issue by promoting increased surface coverage. Additionally, longer immersion times prior to experimentation might also lead to more surface coverage, especially if the adsorption process is slow.

2.4. Conclusions

In this work, the performance of eight different organic corrosion inhibitors (Fig. 2.1) exposed to mild steel substrate was investigated by electrochemical characterization techniques, including potentiodynamic scanning (PDS), linear polarization resistance (LPR) and electrochemical impedance spectroscopy (EIS). PDS analysis was utilized to study the active anodic and cathodic corrosion behavior and passivation range for each inhibitor system, and to obtain Tafel constants specific to each corrosion environment. Results showed slight shifts in cathodic and anodic curves, especially in the passive region, indicating inhibitor effects on the corrosion reaction and their potential influence on the formation of a passivation layer. Extracted Tafel constants displayed little variation in comparison to the control.

LPR experiments in 3.5% (w/v) NaCl were performed in order to investigate steady-state corrosion behavior and to obtain polarization resistance (R_p). Corrosion rates for each inhibitor concentration were calculated using Tafel constants and R_p in order to rank and down-select the eight organic inhibitors by corrosion inhibition efficiency, calculated using Eq. 12. Adrenalone, DOPAC and dopamine progressed through the down-selection process, as they displayed the highest overall corrosion inhibition, reaching 58.3%, 58.2% and 66.8 corrosion inhibition efficiencies, respectively. Additionally, these three inhibitors showed improved performance with increasing concentration, a property consistent with adsorption of the organic molecule to the metal substrate.

Adrenalone, DOPAC and dopamine underwent further electrochemical characterization in 1 M HCl electrolyte. Potentiodynamic scans in acidic conditions revealed a slight shift in the corrosion potential to more active potentials, indicating inhibitor interaction with anodic sites on the metal surface. LPR was performed under these acidic conditions, where adrenalone, DOPAC

and dopamine displayed excellent inhibition properties that improved over time, unlike the comparative inhibitors (ethanolamine, triethanolamine and zinc phthalate additive), which displayed higher corrosion rates as time passed. Maximum inhibition efficiencies were calculated: 95.6% for adrenalone, 90.4% for dopamine and 85.6% for DOPAC. EIS results in 3.5% (w/v) NaCl and 1 M HCl for the down-selected inhibitors proved to be less revealing of mild steel corrosion behavior. This was attributed to the technique directly measuring the impedance of the bare substrate due to incomplete coverage of the surface by the inhibitor molecules.

Overall, experimental results showed that adrenalone, DOPAC and dopamine reduced corrosion rates in 3.5% (w/v) NaCl electrolyte, and exhibited excellent corrosion inhibition for mild steel in 1 M hydrochloric acid. Corrosion rates decreased with increasing concentration, and improved over time. The tests within this method indicated surface adsorption of the molecules on the mild steel surface and were capable of ranking the corrosion inhibition performance. Furthermore, the arrangement of electrochemical tests presented in this methodology proved effective for screening a large selection of chemicals for use as corrosion inhibitors. Furthermore, the test protocol can be easily adapted for investigation of different electrolytes or metal substrates.

2.5. References

(1) ASTM. *ASTM Int.* **2015**, *89* (Reapproved 2015), 1–7.

(2) Jones, D. A. *Principles and Prevention of Corrosion*, 2nd ed.; Prentice Hall: Upper Saddle River, NJ, 1996.

(3) McCafferty, E. *Corros. Sci.* **2005**, *47*, 3202–3215.

(4) *Corrosion Engineering Handbook*; Schweitzer, P. A., Ed.; Marcel Dekker, Inc., 1996; Vol. 1.

(5) Lee, H.-S.; Ryu, H.-S.; Park, W.-J.; Ismail, M. *Materials (Basel)*. **2015**, *8* (1), 251–269.

(6) Ryu, H. S.; Singh, J. K.; Yang, H. M.; Lee, H. S.; Ismail, M. A. *Constr. Build. Mater.* **2016**, *114*, 223–231.

(7) Malel, E.; Shalev, D. E. *J. Chem. Educ.* **2013**, *90* (4), 490–494.

(8) Enos, D. G.; Scribner, L. L. *Cent. Electrochem. Sci. Eng.* **1997**, 1–13.

(9) Wagner, C.; Traud, Z. *Z. Elektrochem.* **1938**, *44*, 391.

(10) Wagner, C.; Traud, W.; Mansfeld. F. *Corrosion* **2006**, *62* (10), 843–855.

(11) Bonhoeffer, K. F.; Jena, W. *Z. Elektrochem.* **1951**, *55*, 151–154.

(12) Stern, M.; Geary, A. L. *J. Electrochem. Soc.* **1957**, *104* (1), 56–63.

(13) Frankel, G. S. *J. ASTM Int.* **2008**, *5* (2), 1–27.

(14) McCafferty, E. *Introduction to Corrosion Science*; 2010.

(15) Mansfeld, F. *J. Solid State Electrochem.* **2009**, *13*, 515–520.

(16) Scully, J. R. *Corrosion* **2000**, *56* (2), 199–218.

(17) ASTM. *ASTM Int.* **2014**, *97*, 1–4.

(18) Liu, Z.; Yu, L.; Li, Q. *J. Wuhan Univ. Technol. Sci. Ed.* **2015**, *30* (2), 325–330.

(19) Myrdal, R. *Corrosion Inhibitors – State of the art*; 2010.

(20) Sanyal, B. *Prog. Org. Coatings* **1981**, *9* (2), 165–236.

(21) Saji, V. S. *Recent Patents Corros. Sci.* **2010**, *2* (1), 6–12.

(22) *Analytical methods in corrosion science and technology*; Marcus, P., Mansfeld, F., Eds.; Taylor & Fancis: Boca Raton, FL, 2006.

(23) Hu, K.; Zhuang, J.; Ding, J.; Ma, Z.; Wang, F.; Zeng, X. *Corros. Sci.* **2017**, *125*, 68–76.

(24) Nagiub, A. M.; Mahross, M. H.; Khalil, H. F. Y.; Mahran, B. N. A. **2013**, *31* (2), 119–139.

(25) Shahid, M. *Adv. Nat. Sci. Nanosci. Nanotechnol.* **2011**, *2*, 1–6.

(26) Enos, D. G.; Scribner, L. L. *The Potentiodynamic Polarization Scan Technical Report 33*; Hampshire, 1997.

(27) Poorqasemi, E.; Abootalebi, O.; Peikari, M.; Haqdar, F. *Corros. Sci.* **2009**, *51* (5), 1043–1054.

(28) *Linear Polarization Resistance and Corrosion Rate*; Durham, NC, 2016.

(29) Amin, M. A.; Khaled, K. F.; Fadl-Allah, S. A. *Corros. Sci.* **2010**, *52* (1), 140–151.

(30) M. Tullmin. *Linear Polarization Resistance*; 2001.

(31) Tian, H.; Li, W.; Wang, D.; Hou, B. *Wuli Huaxue Xuebao/ Acta Phys. - Chim. Sin.* **2012**, *28* (1), 137–145.

(32) Kaya, S.; Tüzün, B.; Kaya, C.; Obot, I. B. *J. Taiwan Inst. Chem. Eng.* **2016**, *58*, 528–535.

(33) Asipita, S. A.; Ismail, M.; Majid, M. Z. A.; Majid, Z. A.; Abdullah, C.; Mirza, J. *J. Clean. Prod.* **2014**, *67*, 139–146.

(34) Singh, A.; Ebenso, E. E.; Quraishi, M. A. *Int. J. Corros.* **2012**, *2012*.

(35) Chigondo, M.; Chigondo, F. *J. Chem.* **2016**, *2016*.

(36) Vinod Kumar, K. P.; Sankara Narayanan Pillai, M.; Rexin Thusnavis, G. *J. Mater. Sci.* **2011**, *46* (15), 5208–5215.

(37) Loto, C. A.; Loto, R. T.; Popoola, A. P. I. *Int. J. Electrochem. Sci.* **2011**, *6* (September), 3830–3843.

(38) Afia, L.; Salghi, R.; Benali, O.; Jodeh, S.; Warad, I.; Ebenso, E.; Hammouti, B. *Port. Electrochim. Acta* **2015**, *33* (3), 137–152.

(39) Gerengi, H.; Sahin, H. I. *Ind. Eng. Chem. Res* **2012**, *51*, 780–787.

(40) Olusegun, A. K.; Oforka, N. C.; Ebenso, E. E. *J. Corros. Sci. Eng.* **2004**, *8* (5), 315–324.

(41) Ji, G.; Anjum, S.; Sundaram, S.; Prakash, R. *Corros. Sci.* **2015**, *90*, 107–117.

(42) Lahhit, N.; Bouyanzer, A.; Desjobert, J.-M.; Hammouti, B.; Salghi, R.; Costa, J.; Jama, C.; Bentiss, F.; Majidi, L. *Port. Electrochim. Acta* **2011**, *29* (2), 127–138.

(43) Tourabi, M.; Nohair, K.; Traisnel, M.; Jama, C.; Bentiss, F. *Corros. Sci.* **2013**, *75*, 123–133.

(44) Boumhara, K.; Tabyaoui, M.; Jama, C.; Bentiss, F. *J. Ind. Eng. Chem.* **2015**, *29*, 146–155.

(45) Sin, H. L. Y.; Umeda, M.; Shironita, S.; Rahim, A. A.; Saad, B. *Res. Chem. Intermed.* **2017**, *43* (3), 1919–1934.

(46) Chennappan, K.; Sethuraman, M. G. *Ind. Eng. Chem. Res.* **2012**, *51*, 10399–10407.

(47) Hussin, M. H.; Kassim, M. J. *Mater. Chem. Phys.* **2011**, *125*, 461–468.

(48) Odewunmi, N. A.; Umoren, S. A.; Gasem, Z. M. *J. Environ. Chem. Eng.* **2015**, *3*, 286–296.

(49) Gürten, A. A.; Keleş, H.; Bayol, E.; Kandemirli, F. *J. Ind. Eng. Chem.* **2015**, *27*, 68–78.

(50) Akrout, H.; Bousselmi, L.; Maximovitch, S.; Triki, E.; Dalard, F. *J. Mater. Sci.* **2012**, *47* (23), 8085–8093.

(51) *Heucorin® FR*; Langelsheim, 2014.

(52) Jeyaprabha, C.; Sathiyanarayanan, S.; Venkatachari, G. *Appl. Surf. Sci.* **2005**, *246*, 108–116.

(53) Brug, G. J.; van den Eeden, A. L. G.; Sluyters-Rehbach, M.; Sluyters, J. H. *J. Electroanal. Chem. Interfacial Electrochem.* **1984**, *176* (1–2), 275–295.

CHAPTER 3. SURFACE CHARACTERIZATION PROCEDURE FOR ORGANIC MOLECULES AS CORROSION INHIBITORS ON MILD STEEL

3.1. Abstract

In order to investigate the surface adsorption characteristics of the inhibitor molecules, X-ray photoelectron spectroscopy (XPS) and quartz crystal microbalance (QCM) experiments were performed. XPS was performed on steel samples that were immersed in 20 mM solutions of 3,4-dihydroxyphenylacetic acid (DOPAC), adrenalone HCl and dopamine HCl. QCM tests were run on Au-coated quartz crystals with 20 mM and 10 mM solutions of these same inhibitors in 3.5% (w/v) NaCl. In order to directly track adsorption on the electrode surface, the change in resonant frequency of the quartz crystal was directly correlated to a change in mass using the Sauerbrey equation. XPS spectra indicate adsorption of inhibitor molecules to the mild steel surface; rinsing these samples for 10 seconds under a stream of 18 MΩ ultra-pure water resulted in a loss of inhibitor signals in the XPS spectra. Results of the QCM experiments showed positive mass change on the electrode surface, indicating that the inhibitors adsorb onto the gold surface. 20 mM inhibitor concentrations displayed higher mass adsorptions than 10 mM counterparts. Molecular weight of the inhibitor species also appeared to be directly related to mass adsorption, following the trend: adrenalone > DOPAC > dopamine, at 20 mM inhibitor concentration.

3.2. Experimental

3.2.1. X-ray Photoelectron Spectroscopy (XPS)

In order to confirm that the organic inhibitors adsorb to the carbon steel substrate, a reliable and precise surface characterization technique is required. X-ray photoelectron spectroscopy offers the precision necessary to detect monolayers of molecules and is capable of quantitative elemental analysis at the metallic surface, an aspect that proves useful when trying to confirm the presence

or absence of inhibitors or corrosion products on substrates in corrosion applications. Unfortunately, the procedure requires ultrahigh vacuum conditions so in situ investigations are not available, but the procedure still offers a means to detect chemicals present on the metal surface.

The standard XPS experiment bombards the metallic surface with an incident X-ray beam, ionizing the atoms of the top few nm of the surface. This causes electrons (primarily from the inner core levels) of these elements to be ejected from the sample. These electrons have a distinct energy depending on which chemical element it originates from; instrument detectors collect these electrons and analyze their binding energy to determine which element they were ejected from. XPS data is typically presented as a plot depicting the number of electrons detected against binding energy of these electrons; peaks on the plot are then directly correlated to elements present on the surface. In this work, XPS was used to identify the presence or absence of inhibitor molecules by evaluating the spectra for marker elements specific to the organic inhibitors.

The inhibitor solutions for this experiment were prepared using 18 MΩ ultra-pure water; chemicals from Sigma-Aldrich. Solutions were prepared at 20 mM concentration and were devoid of NaCl or HCl (which had been used in previous experiments). Q-Panel R-36 steel substrates were cut into 3/8" x 3/8" squares with a little tab left on one edge for handling with tweezers. The front and back faces of the substrates were sanded with 400-grit silicon carbide sandpaper and then placed under a stream of N_2 gas to clear off remaining sanding debris. The samples were rinsed with acetone and dried once again under a stream of N_2 gas prior to inhibitor exposure.

These prepared substrates were immersed into the inhibitor solutions and remained totally submerged for 30 minutes. Immediately upon removal, the substrates were either dried under a stream of N_2 gas, or rinsed with 18 MΩ ultra-pure water for ten seconds. The samples were then dried with N_2 gas and stored overnight in a desiccator prior to XPS testing. XPS spectra were

measured with a Thermo Scientific K-Alpha XPS system, using a monochromated Al K_α X-ray source (1486.6 eV) on a 400 μm spot size. 5 survey passes were performed on each sample at a pass energy of 200 eV, with a step size of 1 eV.

3.2.2. Quartz Crystal Microbalance (QCM)

Small changes in mass on the surface of on an electrode can be measured using a quartz crystal microbalance (QCM), which is an instrument consisting of a thin crystal made of quartz, that is plated with an electrode on both sides. The instrument functions based on the piezoelectric effect, which is induced by the application of an alternating potential and leads to oscillation of the crystal. A standing shear wave is formed at a potential specific to the quartz type; this is known as the resonant frequency, which is very sensitive to mass deposition. Changes in resonant frequency, as a result of a damping effect, can be directly related to changes in mass using the Sauerbrey equation:[1]

$$\Delta f = -\left(\frac{2f_o^2}{A\sqrt{\rho_q \mu_q}}\right)\Delta m \qquad \text{(Eq. 20)}$$

where f_o is the resonant frequency, Δm is the change in mass, A is the piezoelectrically active area of the electrode, and ρ_q and μ_q are the density and shear modulus of the quartz, respectively. Application of this equation requires the assumption that the deposited material is rigid. Deposition of viscous materials introduces more complexity that can be accounted for by introducing another term to Eq. 20, however that is beyond the scope of this work as it was assumed the inhibitor molecules are sufficiently rigid. Further manipulation of the Sauerbrey equation yields:

$$\Delta f = -C_f \Delta m \qquad \text{(Eq. 21)}$$

where C_f is the crystal calibration constant. Because the crystal calibration constant is typically supplied by the manufacturer, this equation becomes relatively straightforward in relating the measured change in frequency to a change in mass on the electrode surface.

The quartz crystal microbalance is capable of nanogram resolution in its measurements, which is more than sufficient for observing monolayer development on the electrode surface.[2] Because of this immense sensitivity, QCM instruments are utilized in research investigating such topics as layer-by-layer (LbL) assembly, protein-substrate interactions and biofilm growth, formation of metal oxides and metal dissolution, conductive polymers and, of course, corrosion inhibitors.[3–11] The technique is actually well suited for inhibitor studies, as it is operable in solution and provides a metallic electrode surface for adsorption to take place, mimicking the same conditions of electrochemical inhibitor studies. Furthermore, the instrument's mass detection sensitivity is accurate enough to detect a single layer of adsorbed organic molecules. In this work, the quartz crystal microbalance was utilized to identify mass changes on the electrode surface to investigate the surface adsorption characteristics of the organic inhibitors.

A Gamry Instruments eQCM 10M quartz crystal microbalance was used for all QCM experiments. Measurements took place within a static polytetrafluoroethylene cell using 10-Mhz Au-coated quartz crystals with a 0.209 cm^2 electroactive area and 226 $Hz \cdot cm^2/\mu g$ factory calibration factor. A schematic of the QCM setup is shown in Figure 3.1.

In addition to a blank control solution, 3,4-dihydroxyphenylacetic acid, adrenalone HCl, and dopamine HCl at 10 mM and 20 mM concentrations were investigated. Prior to starting data collection, the QCM cell was filled with 3.5% (w/v) NaCl solution. Once the readings stabilized (typically 5-10 minutes) a concentrated inhibitor solution was added to the cell while data collection continued, bringing the solution to the desired inhibitor concentration (either 10 mM or

20 mM). Measurements were then performed until stabilization occurred again and continued for an additional 300 seconds.

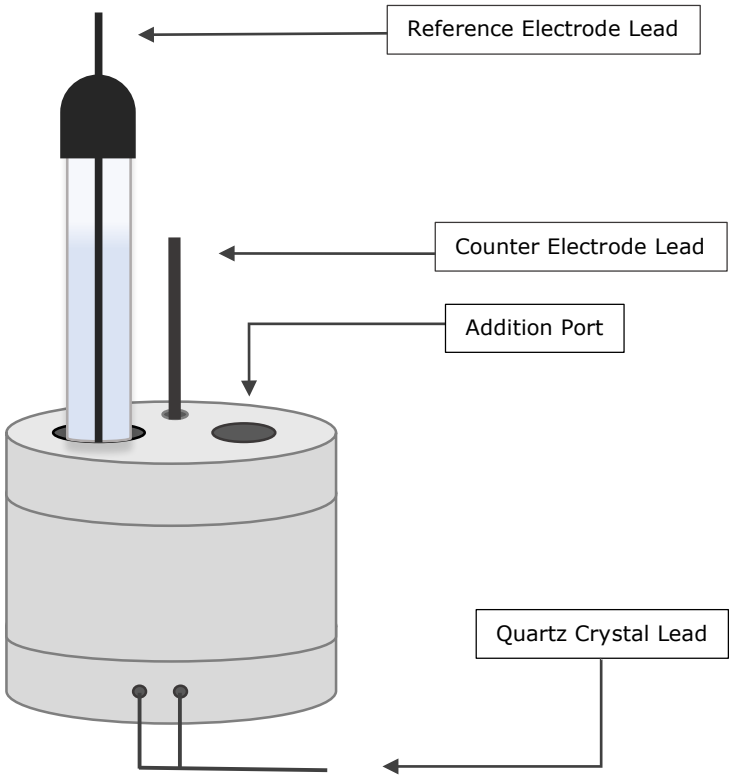

Figure 3.1. Schematic of the QCM cell. The quartz crystal lead attaches to the QCM instrument and to the working electrode of the potentiostat.

3.3. Results and Discussion

3.3.1. X-ray Photoelectron Spectroscopy (XPS)

X-ray photoelectron spectroscopy was performed in order to detect the presence of inhibitor molecules at the steel substrate interface at the elemental level. Survey scans of each inhibitor system under rinsed and unrinsed conditions indicated which elements were present and curve analysis was performed in order to quantify elemental presence as a function of total percent. Figure 3.2 and Figure 3.3 show XPS survey scans of the unrinsed and rinsed mild steel samples, the curves were generated from raw data without further manipulation. Spectral analysis software

supplied by Thermo Scientific was used for curve fitting and integration of element peaks to generate atomic percent (%) data displayed in Table 3.1. In order to preserve the delicate adsorptive interaction of the inhibitors with the surface, ion sputtering cleaning was not performed on the samples prior to XPS measurements, therefore oxygen and carbon contamination from the atmosphere contributed to overall O1s and C1s peak intensities.

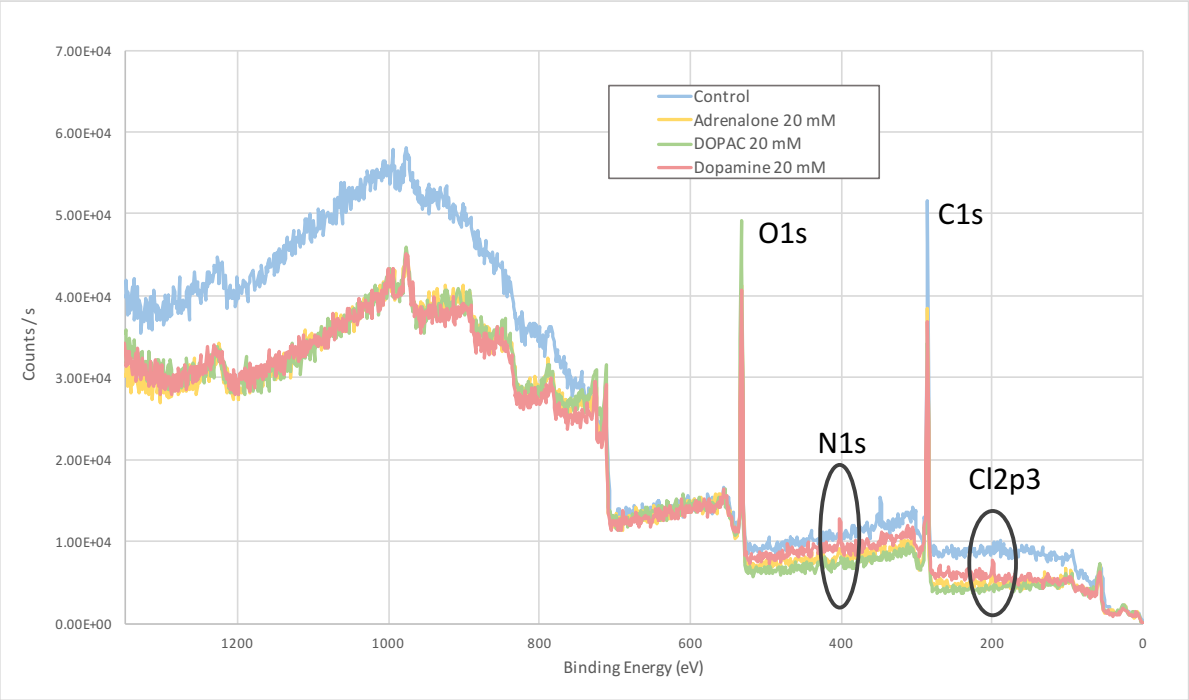

Figure 3.2. XPS survey spectra of unrinsed mild steel samples exposed to 20 mM inhibitor solutions.

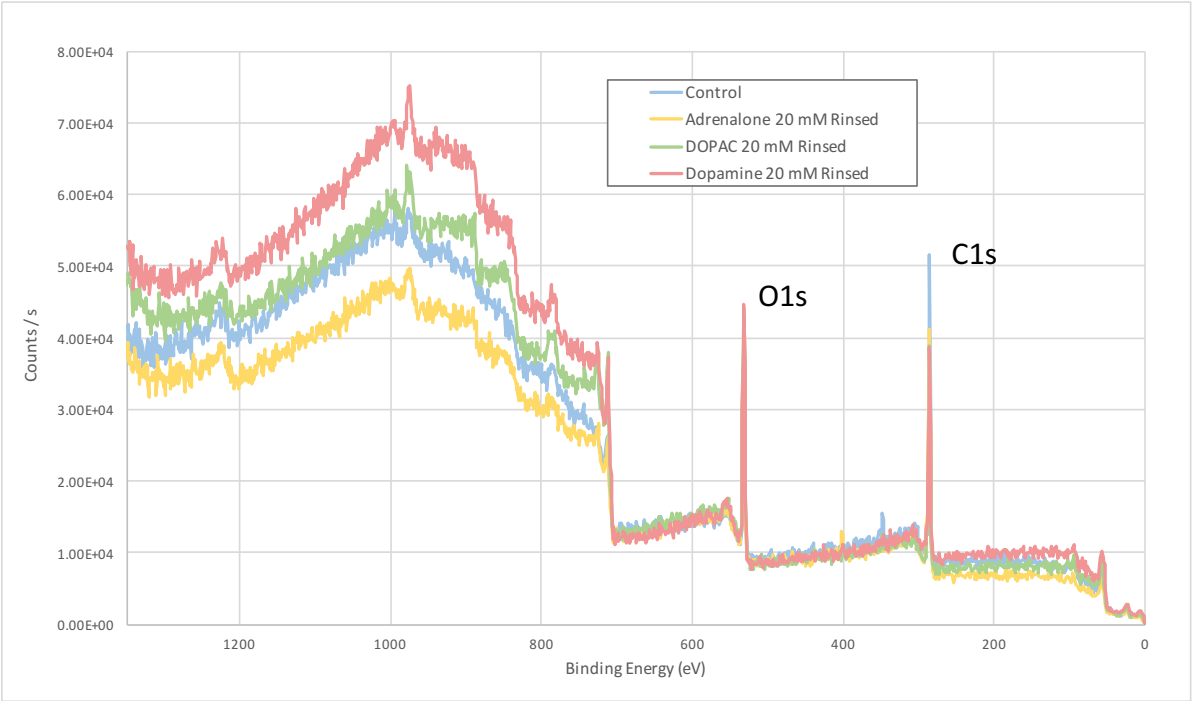

Figure 3.3. XPS survey spectra of rinsed mild steel samples exposed to 20 mM inhibitor solutions.

The peak intensities of the control sample for C1s and O1s were significant due to atmospheric contamination during transfer of the samples from the blank solution to the XPS vacuum chamber. Because the organic molecules are comprised mainly of carbon, utilizing this peak for detection of the inhibitor proved somewhat difficult, a drawback also described by Kern and Landolt, who opted to use a Br-tagged organic molecule for detection.[11] However, as shown in Figure 3.4, The O1s peak displayed notable differences in signal intensity for each unrinsed sample exposed to inhibitor solution in comparison to the control. Peak intensity is significantly higher for the samples exposed to the inhibitor solutions, with DOPAC displaying the largest; the calculated atomic percent for O1s signal is 36.84% for DOPAC, 28.86% for adrenalone and 27.01% for dopamine. The trend follows the oxygen content for each inhibitor: DOPAC contains 4 oxygen atoms per molecule, compared to just 2 for dopamine and 3 for adrenalone.

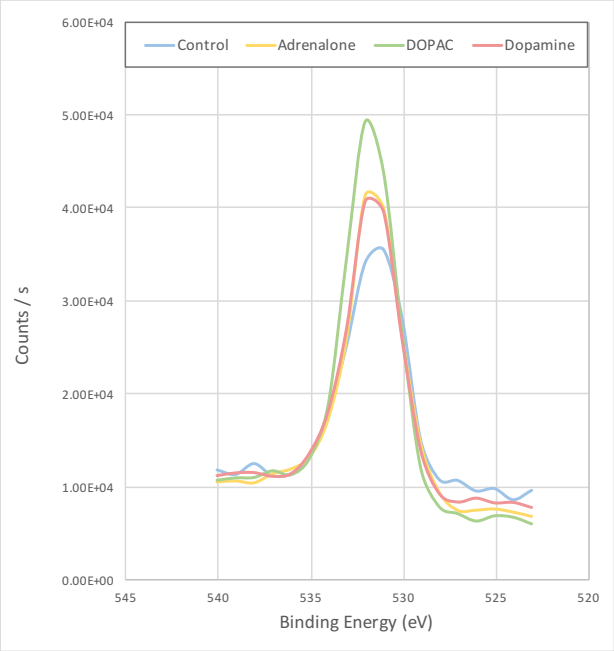

Figure 3.4. XPS spectra of O1s peaks corresponding to unrinsed samples exposed to 20 mM inhibitor solutions.

More suggestive of inhibitor adsorption, though, is the presence of N1s and Cl2p3 peaks in the XPS spectra for the unrinsed adrenalone and dopamine samples, specifically marked in Figure 3.2 at binding energies of about 400 eV and 200 eV, respectively. Dopamine and adrenalone contain an amine within their tail structure and were synthesized and shipped as hydrochloride salts, so these signals would be expected for adsorbed inhibitor species. Furthermore, Tian et al. observed similar results with a different organic inhibitor system containing a nitrogen constituent, attributing the presence of the N1s peak to a chemically coordinated N atom bonded to the substrate.[12] This suggests that adsorption is occurring through the tail structure, rather than the coordinating-prone catechol structure. Although chlorine is not chemically bonded to either dopamine or adrenalone, its presence on the substrate surface is not surprising as a contaminant. Both the N1s and Cl2p3 signals disappear upon rinsing (Figure 3.3). The fact that the force of flowing water was able to reduce the signal and essentially eliminate the identifying elements (N

within the molecule, and Cl as a secondary marker), suggests that the inhibitors were weakly adsorbed to the mild steel surface.

It is assumed that adsorption of organic molecules occurs through one of two mechanisms, either electrostatic interaction between the charged metal surface and charged species in solution, or through chemisorption of the organic molecules to the substrate by sharing or donating electron constituents.[13–19] Physisorption has largely been associated with the first mechanism and is the weaker interaction, whereas chemisorption has been used to describe the stronger chemical bonding interaction described by the sharing of electrons – often the mechanism used to describe organic inhibitor adsorption has been a combination of the two.[20–22] Additionally, several researchers have suggested an interaction between inhibitor molecules and negatively charged acid anions, such as chloride ions, that have been attracted to the positively charged mild steel surface, in a sort of two-step adsorption process that is more characteristic of electrostatic interactions.[21,23] Given the complex nature of the chemicals involved in this work, displaying free electron pairs, π-electrons and supporting chloride ions, each adsorption mechanism is reasonably valid, suggesting a combination of the above.

The rinsed mild steel samples show a slight decrease in the O1s peak when compared to their unrinsed counterparts, however the calculated atomic percents for the O1s signal increase to 37.70% for DOPAC, 33.62% for adrenalone and 37.17% for dopamine. This is probably due to a combination of several factors, including the replacement of inhibitor molecules on the metal surface with water molecules as the inhibitor is rinsed away and the development of a thin layer of oxygen-containing corrosion product.[10,11,17]

Additionally, a Si2p signal appears in the adrenalone sample upon rinsing. Because no silicon is present in any inhibitor or within the steel alloy, it is assumed to be a contaminant

introduced into the experiment sometime between inhibitor application and introduction of the samples into the XPS vacuum chamber.

Table 3.1. XPS elemental peaks calculated as overall atomic percents for inhibitor solutions applied to mild steel.

Sample	Atomic Percent (%)				
	C1s	O1s	N1s	Cl2p3	Si2p
Control	73.39	26.61	-	-	-
Adrenalone	61.01	28.86	7.10	3.03	-
Adrenalone Rinsed	63.17	33.62	-	-	3.21
DOPAC	63.16	36.84	-	-	-
DOPAC Rinsed	62.30	37.70	-	-	-
Dopamine	62.53	27.01	7.07	3.39	-
Dopamine Rinsed	62.83	37.17	-	-	-

3.3.2. Quartz Crystal Microbalance (QCM)

Adsorption experiments using the quartz crystal microbalance revealed a reduction in the resonant frequency for each inhibitor system tested, with higher concentrations yielding lower crystal frequencies. The reduction in frequency is assumed to be entirely attributed to the introduction of inhibitor molecules and subsequent adsorption, as the control solution displayed no change in frequency during the duration of the experiment. These results can be directly converted into a change in mass using the modified Sauerbrey equation (Eq. 21). QCM plots for calculated mass change as a function of time for each inhibitor system is displayed in Figure 3.5. These curves were normalized with regard to mass change so that they could be easily compared to one another; furthermore, portions of the graph corresponding to frequency stabilization prior to inhibitor addition have been cropped for clarity. The addition of inhibitor to each system is indicated by the large spikes in mass at about 125 s. Subsequent stabilization is seen as the curves reach a plateau within the following 100-200 seconds.

Results indicate that 20 mM inhibitor concentrations led to greater mass gain on the electrode surface in comparison to 10 mM concentrations of the same corrosion inhibitor This suggests there is increased surface coverage at higher inhibitor concentrations, potentially leading to better corrosion inhibition by blocking exposed anodic and cathodic sites on actively corroding metal substrates. The higher rate of adsorption also suggests that total surface coverage of the electrode may not have been reached, as more inhibitor clearly was able to adsorb to the substrate. Further studies that incorporate a stepwise addition of inhibitor might be performed in order to determine the surface saturation point when the entire surface is covered.

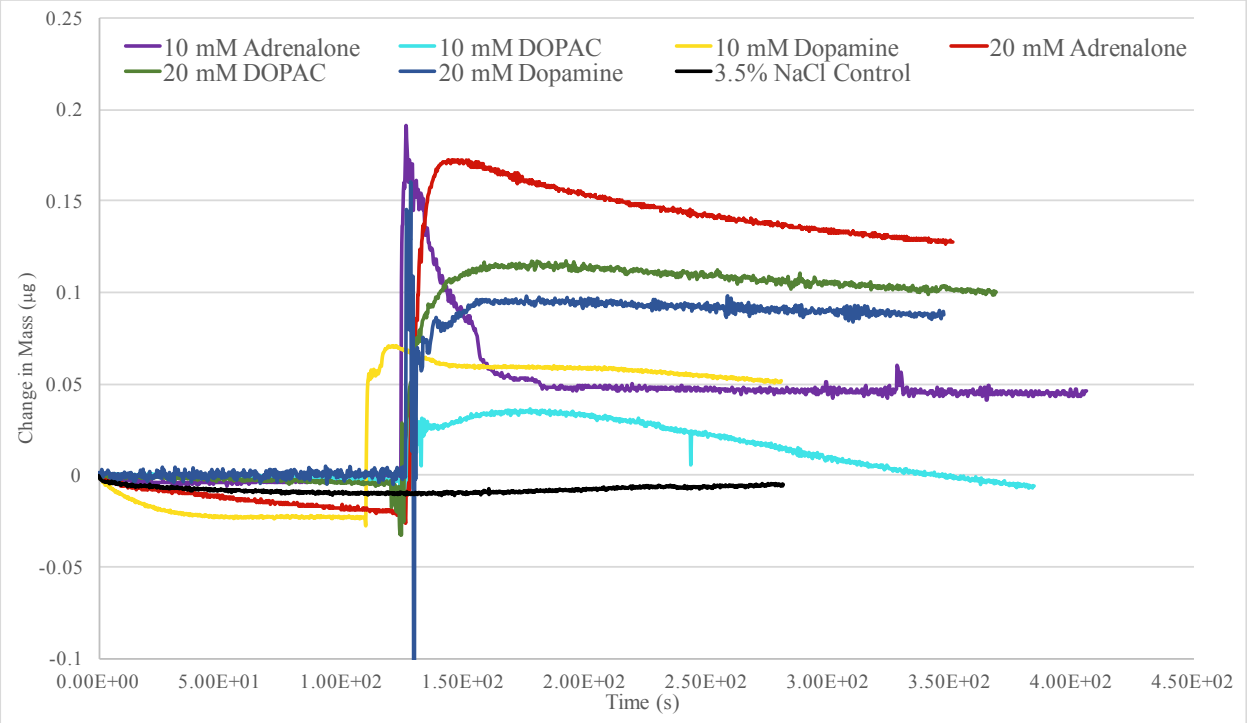

Figure 3.5. Mass change plotted against time for inhibitors at 10 mM and 20 mM concentrations on Au-coated quartz crystal.

In the case of 10 mM DOPAC concentrations, each replicate tended to show an initial mass gain followed by a slow decay back to the unloaded control state. This may indicate that a threshold exists where an adsorptive layer of molecules does not stabilize on the surface when applied at

concentrations below this threshold, instead forming a sort of pseudo protective layer initially when local inhibitor concentrations are significantly higher than the bulk concentration. A decay off the surface would then occur as local concentrations drift towards the bulk concentration, below the proposed threshold concentration. Further studies, perhaps one similar to the investigation performed by Kern and Landolt, where QCM was performed with stepwise addition of the inhibitor, would need to confirm this proposed mechanism.[11]

Some of the noise in the QCM data is due to user error, but these artifacts quickly disappeared as the frequency decayed to its stabilized state. A summary of the QCM results is displayed in Figure 3.6. Average mass gain is calculated from three replicates, with values extracted from the stabilized portion of the curve. For the 10 mM DOPAC tests, values were extracted from the initial mass loading, prior to signal decay.

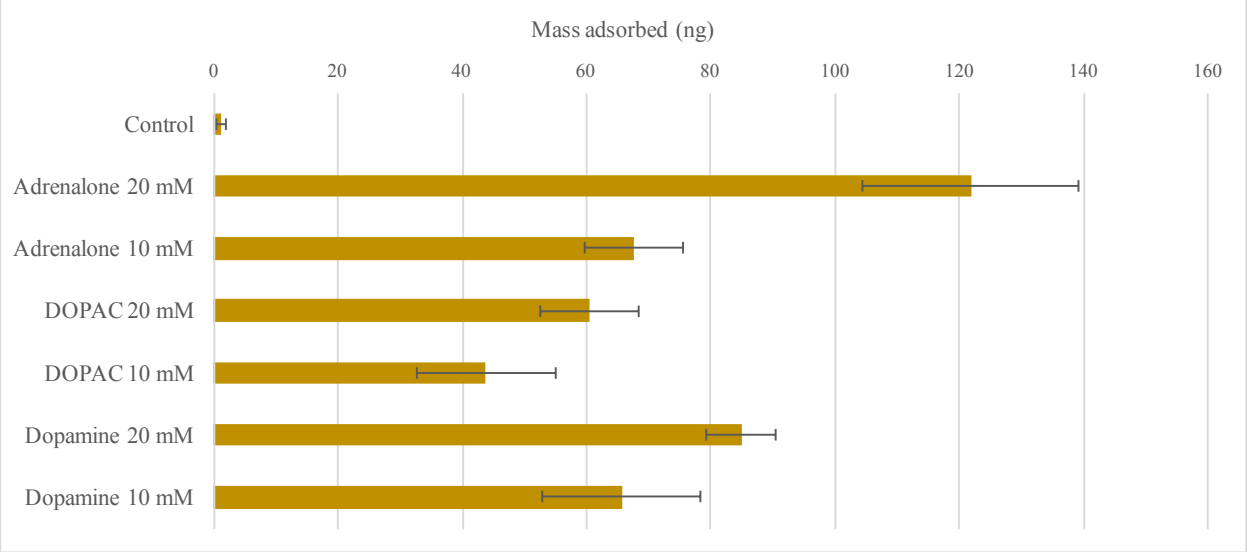

Figure 3.6. Average mass gain on Au-coated quartz crystal for each inhibitor system.

At 20 mM concentrations, adrenalone, dopamine and DOPAC displayed average reductions in crystal frequency translating to 121.8 ng, 84.9 ng and 60.52 ng of adsorbed mass, following the trend of molecular weight for each molecule. Intuitively, this makes sense if it is

assumed that each inhibitor has equal surface coverage on the substrate. However, a perfectly linear relationship is not observed, as seen in Figure 3.7, indicating varying degrees of surface coverage for each inhibitor. DOPAC shows slightly less surface coverage when compared to adrenalone and dopamine. Dopamine and adrenalone both contain a nitrogen constituent along its tail structure, which may facilitate hydrogen bonding between neighboring molecules on the substrate surface, perhaps explaining their slightly improved surface adsorption at either concentration when compared to DOPAC, which lacks nitrogen. This proposed interaction seems even more compelling considering the catechol structure of these molecules has an affinity for adsorption to a variety of metallic substrates, including iron, aluminum, manganese, zinc and titanium.[24–27] This hypothesized mechanism positions the nitrogen-containing tail structures away from the surface and in close proximity with one another, facilitating possible hydrogen bonding.

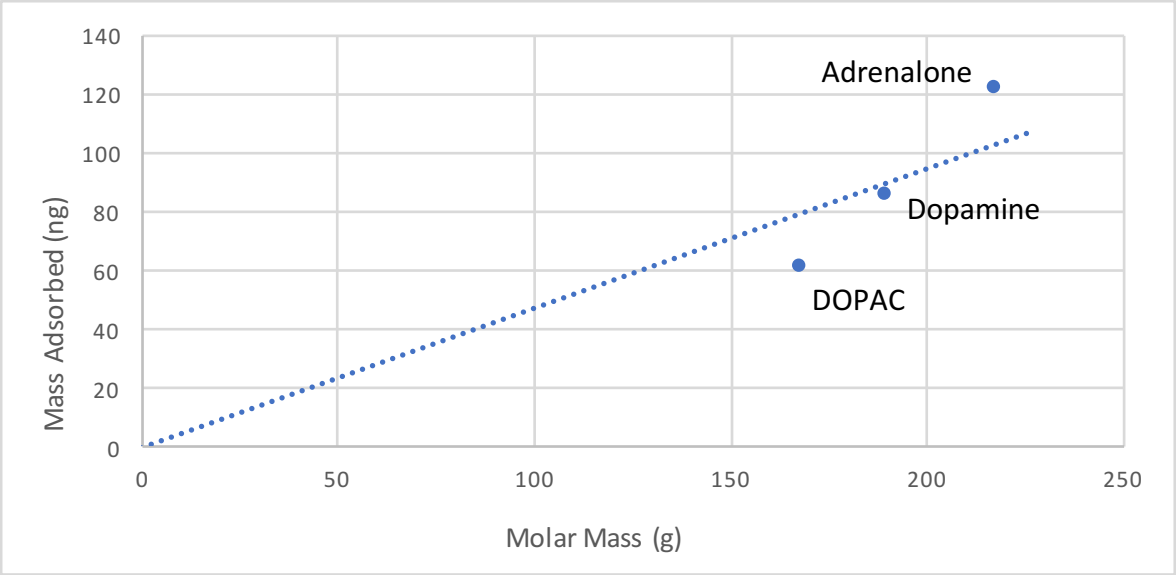

Figure 3.7. Molar mass vs. mass adsorbed to the Au-coated quartz crystal for 20 mM inhibitor concentrations.

One caveat with the quartz crystal microbalance study is that the substrate utilized to track surface adsorption is not mild steel. Instead the quartz crystals are gold plated and offer a stipulated

comparison to mild steel surfaces. Several differences between the two substrates that might have immediate impact on the adsorption mechanisms of organic inhibitors include electronic structure, crystalline structure (FCC vs. BCC), atomic radius and the potential of the metal.[9] These properties will have direct impact on the adsorption mechanisms and possible steric or electrostatic interactions between the organic molecule and the individual metal atoms. Additionally, the heterogeneity of the surface, in terms of exposed anodic and cathodic sites, will have an impact.[11] For example, gold essentially remains inert in the tested solution in comparison to iron, which has a much more complex surface of cathodic and anodic sites, in addition to corrosion product build-up – these effects will also impact the adsorption mechanism and the strength of interaction. In one study by Kern and Landolt, the adsorption of a carboxylic acid-based organic inhibitor to gold and iron coated surfaces was investigated in order to study the differences in energy of adsorption between the two.[9] They concluded that the interaction with iron is slightly greater than with gold, suggesting the use of gold for adsorption studies might underestimate the free energy of adsorption of organic inhibitors on iron. Several other studies found similar results, indicating inhibitor interactions to be stronger with iron substrates than gold.[28,29] Although these works suggest the organic molecules investigated in the present study with the Au-coated quartz crystal might show larger interactions to an Fe-coated crystal, further studies should be performed with an Fe-coated quartz crystal in order to corroborate these findings.

3.4. Conclusions

In this work, investigation of physical substrate-inhibitor interactions was performed using X-ray photoelectron spectroscopy (XPS) and quartz crystal microbalance (QCM) experiments. XPS analysis revealed detection of inhibitor constituents on the mild steel surface, confirming the adsorption of the molecules. Additionally, the loss of identifying elemental peaks N1s and Cl2p3

in adrenalone and dopamine samples upon rinsing the samples with 18 MΩ ultra-pure water further suggests the adsorptive behavior of these organic inhibitor. XPS investigation of organic inhibitors offers valuable surface detection capabilities on substrate surfaces, however analysis of results is made easier if marker elements are incorporated into the molecular structure such as nitrogen, like in the case of adrenalone and dopamine.

Adsorption of each organic inhibitor was confirmed through the QCM technique. Experiments performed on an Au-coated quartz crystal in 20 mM and 10 mM concentrations of adrenalone, dopamine and DOPAC in 3.5% (w/v) NaCl showed that adsorption of inhibitor molecules leads to a decrease in resonant frequency of the quartz crystal. A frequency decrease corresponds to a mass increase on the substrate surface, confirming the adsorption process of the inhibitors. 20 mM inhibitor concentrations led to greater mass gain on the electrode surface in comparison to 10 mM concentrations, indicating increased surface coverage of the Au-plated quartz crystal. These results suggest improved inhibitor performance can be attained at higher concentrations due to more anodic and cathodic sites being blocked on an actively corroding metal substrate. The initial mass gain displayed for 10 mM DOPAC samples appeared to decay after initial adsorption, suggesting there might be a critical inhibitor concentration necessary for a stable layer to form on the substrate. Although the Au-coated surface is not a perfect substitute for mild steel, these results suggest that an adsorption mechanism for protection of the surface against corrosion, as suggested from electrochemical characterization results, is valid. Further QCM studies on Fe-coated crystals should be performed in order to corroborate these findings.

These results display the sensitivity of the QCM instrument to exceedingly small mass changes on a substrate surface, a requirement for investigations involving thin layer adsorption. Furthermore, the interpretation of results is unambiguous, clearly showing frequency shifts of the

quartz crystal in real time as the experiment proceeds. It is for these capabilities that QCM investigations have become such an integral part of surface characterization for corrosion inhibitors and their interaction with metal substrates.

3.5. References

(1) Sauerbrey, G. *Zeitschrift fur Phys.* **1959**, *155* (2), 206–222.

(2) *Analytical methods in corrosion science and technology*; Marcus, P., Mansfeld, F., Eds.; Taylor & Fancis: Boca Raton, FL, 2006.

(3) Hillman, A. R. *J. Solid State Electrochem.* **2011**, *15*, 1647–1660.

(4) Marshakov, A. I.; Rybkina, A. A.; Maksaeva, L. B.; Petrunin, M. A.; Nazarov, A. P. *Prot. Met. Phys. Chem. Surfaces* **2016**, *52* (5), 936–946.

(5) Ithurbide, A.; Frateur, I.; Galtayries, A.; Marcus, P. *Electrochim. Acta* **2007**, *53*, 1337–1346.

(6) *Monitoring layer-by-layer assembly of polyelectrolyte films using a quartz crystal microbalance*; 2016.

(7) Payet, V.; Dini, T.; Brunner, S.; Galtayries, A.; Frateur, I.; Marcus, P. *Surf. Interface Anal.* **2010**, *42* (6–7), 457–461.

(8) Ogle, K.; Weber, S. **2000**, *147* (5), 1770–1780.

(9) Kern, P.; Landolt, D. *J. Electrochem. Soc.* **2001**, *148*, B228–B235.

(10) Kern, P.; Landolt, D. *Electrochim. Acta* **2001**, *47* (4), 589–598.

(11) Kern, P.; Landolt, D. *Corros. Sci.* **2002**, *44* (8), 1809–1824.

(12) Tian, H.; Li, W.; Hou, B.; Wang, D. *Corros. Sci.* **2017**, *117*, 43–58.

(13) McCafferty, E. *Introduction to Corrosion Science*; 2010.

(14) Bozorg, M.; Shahrabi Farahani, T.; Neshati, J.; Chaghazardi, Z.; Mohammadi Ziarani, G. *Ind. Eng. Chem. Res.* **2014**, *53* (11), 4295–4303.

(15) Olusola, J. O.; Oluseyi, A. K.; Kehinde, O. O.; Olayinka, A. O.; Oluwatosin, J. M. *Port. Electrochim. Acta* **2009**, *27* (5), 591–598.

(16) Boumhara, K.; Tabyaoui, M.; Jama, C.; Bentiss, F. *J. Ind. Eng. Chem.* **2015**, *29*, 146–155.

(17) Tian, H. W.; Li, W. H.; Wang, D. P.; Hou, B. R. *Wuli Huaxue Xuebao/ Acta Phys. - Chim. Sin.* **2012**, *28* (1), 137–145.

(18) Ghareba, S.; Omanovic, S. *Electrochim. Acta* **2011**, *56* (11), 3890–3898.

(19) Fragnani, A.; Trabanelli, G. *Corrosion* **1999**, *55*, 653.

(20) Gürten, A. A.; Keleş, H.; Bayol, E.; Kandemirli, F. *J. Ind. Eng. Chem.* **2015**, *27*, 68–78.

(21) Sin, H. L. Y.; Umeda, M.; Shironita, S.; Rahim, A. A.; Saad, B. *Res. Chem. Intermed.* **2017**, *43* (3), 1919–1934.

(22) Chennappan, K.; Sethuraman, M. G. *Ind. Eng. Chem. Res.* **2012**, *51*, 10399–10407.

(23) Vijayalakshmi, P. R.; Rajalakshmi, R.; Subhashini, S. *Port. Electrochim. Acta* **2011**, *29* (1), 9–21.

(24) Sachin, H. P.; Khan, M. H. M.; Raghavendra, S.; Bhujangaiah, N. S. *Open Electrochem. J.* **2009**, *1* (1), 15–18.

(25) Lefebvre, L. The adsorption characteristics and anticorrosive effects of the adhesive protein of the blue mussel Mytilus edulis, University of Delaware, 1993.

(26) Xu, Z. *Sci. Rep.* **2013**, *3*, 1–7.

(27) Ata, M. S.; Liu, Y.; Zhitomirsky, I. *RSC Adv.* **2014**, *4* (43), 22716.

(28) Akrout, H.; Bousselmi, L.; Maximovitch, S.; Triki, E.; Dalard, F. *J. Mater. Sci.* **2012**, *47* (23), 8085–8093.

(29) Olsson, C. O. A.; Leonard, D.; Agarwal, P.; Mathieu, H. J.; Landolt, D. In *Proceedings of the 12th International Conference on Secondary Ion Mass Spectrometry*; Buxelles, Belgium, 1999; p 847.

CHAPTER 4. CONCLUSIONS, PROPOSED METHODOLOGY AND FUTURE WORK

4.1. Conclusions

Electrochemical techniques are valuable characterization methods for organic corrosion inhibitor systems applied to metal substrates and can add a great deal of kinetic and thermodynamic information to surface characterization techniques. In this work, a test method involving a screening procedure for organic inhibitors with electrochemical techniques (LPR, PDS and EIS) was developed while evaluating the effectiveness of these chemicals on mild steel substrates in sodium chloride and hydrochloric acid electrolytes.

Eight inhibitors (4-aminosalicylic acid, 5-aminosalicylic acid, adrenalone, allantoin, betaine, diazolidinyl urea, DOPAC and dopamine) were initially screened by OCP monitoring and LPR analysis in NaCl electrolyte, with OCP results suggesting adrenalone, DOPAC and dopamine to have strong interactions with the mild steel substrate. LPR analysis resulted in the highest inhibition efficiencies ($\geq 50\%$) out of all eight initial chemicals for these same inhibitors, indicating good corrosion protection.

Subsequent down-selection of the organic inhibitors led to further LPR evaluation of adrenalone, DOPAC and dopamine in HCl; these results indicate excellent inhibition efficiencies ($\geq 85\%$) and reduced corrosion rates with increasing inhibitor concentration in comparison to uninhibited conditions. Corrosion protection was sustained for the entire duration of the 22 hour LPR test in HCl media. PDS experiments in NaCl and HCl agree with LPR findings, indicating slightly reduced anodic and cathodic currents about the corrosion potential and in the passivation range. EIS results were noisy and less conclusive, yielding polarization resistance values that deviated from LPR results.

XPS analysis of the down-selected inhibitors on mild steel confirmed surface adsorption to the substrate, with rinsed samples showing lack of inhibitor adsorption. QCM tests displayed mass gain to the electrode, indicating adsorption to the Au-coated quartz crystal. These surface characterization results support the proposed adsorption mechanism of corrosion inhibition and are in agreement with electrochemical test results.

The test methodology utilized in this work was capable of screening eight potential organic corrosion inhibitors, narrowing the potential collection of inhibitors to the three most-promising chemicals and producing a detailed evaluation of them through electrochemical techniques and surface characterization experiments. In addition to saving time, the process also saved labor and experimentation costs that would have went towards extended evaluation of the other five chemicals, all of which were screened out of the project early in the test methodology. This allows more promising molecules to be identified quicker, which is precisely the goal when trying to probe the library of organic chemicals for effective corrosion inhibitors.

4.2. Proposed Method

Current research is focused on investigating environmentally-friendly, organic inhibitors as replacements to toxic, inorganic inhibitors. Many of these green inhibitors are sourced from plant extracts or are derived from pharmaceuticals, which generates a huge population of potential chemical candidates. In a large selection of literature, electrochemical characterization of an organic inhibitor often involves the determination of its effect on the metal corrosion rate through several methods, including LPR, EIS and PDS, however studies are usually limited to investigation of one or two molecules or a single plant extract, at various concentrations. The central purpose of the presented work is the development of a uniform characterization method for organic corrosion inhibitors, especially with the intention of incorporating a screening method capable of analyzing

the inhibition performance of a large group of chemicals prior to more detailed investigation. The initial inhibitor screening process is an essential step in the proposed method because its purpose is to save time and expedite the process of inhibitor evaluation. Ensuring that effective inhibitors are selected for further characterization and ineffective ones are trimmed from the candidate population is critical for successful implementation.

Because effectiveness of inhibitors is directly reflective of their ability to suppress corrosion rates, determining the corrosion rate of inhibitor systems became the most important aspect of developing the test methodology. Linear polarization resistance is a quick way to reliably determine corrosion rates, especially if Tafel constants can be assumed for a particular substrate-electrolyte system, which alleviates the need for additional PDS tests specifically used for elucidating β_a and β_c. In this work, separate PDS experiments were performed in order to obtain actual Tafel constants for each inhibitor system so that a recommendation could be made as to whether this has to be done, or if assuming Tafel constants is acceptable. Results showed little variation in β_a and β_c; furthermore, corrosion rate calculation shows little sensitivity to changes in these values.

Based on these findings, performing an entirely separate set of experiments to obtain Tafel constants for corrosion rate calculations is not recommended especially considering this process doubles the initial amount of research efforts for a method designed to streamline corrosion inhibitor discovery. Instead, assumptions for these values based on previous literature is acceptable for a screening method.

The overall recommended procedure for electrochemical characterization of organic inhibitors and the down-selection criterion are as follows:

1. Substrate and inhibitor electrolyte preparation that is consistent across experiments.

2. Linear polarization resistance testing incorporating a 1 hour stabilization period monitoring the open circuit potential prior to test commencement. LPR scan rate of 0.1666 mV/s from ±10 mV about E_{corr}. Testing occurring intermittently over a three-week period.

3. LPR data analysis to obtain electrochemical system descriptors, especially polarization resistance, R_p.

4. Calculation of corrosion rates based on assumed Tafel constant values and R_p obtained from LPR analysis.

5. Ranking of inhibitors based on calculated corrosion rates, and subsequent down-selection of inhibitors that achieved sustained inhibition efficiencies greater than 50% for the duration of the LPR experiment.

6. Potentiodynamic testing of screened inhibitors to qualitatively evaluate passivation behavior. Polarization (occurring after 1 hour stabilization period) from -1 V to +5 V vs. E_{corr} at a scan rate of 10 mV/s.

7. The EIS procedure requires further studies to devise a better inhibitor application process prior to continued incorporation in this methodology.

8. Additional surface characterization techniques of particular interest to intended applications or for confirmation of electrochemical experimental results (e.g. XPS, QCM, EDS, SEM, weight loss determination).

The presented methodology is distinct from current practices because it incorporates a screening procedure that is notably absent in other research. Most inhibitor studies are

comprehensive in nature, characterizing electrochemical and surface properties of one or two substances entirely, regardless of performance. Incorporating the LPR screening step prevents this unnecessary comprehensive characterization of substances that are relatively ineffective in comparison to more auspicious potential candidates, saving time and money. The screening procedure is centered around the linear polarization resistance technique for several reasons: 1) LPR allows for fast testing, 2) LPR is a non-destructive technique so repeat tests can be done over time, and 3) LPR data analysis reveals corrosion rate information that is needed for determining inhibition efficiencies (%IE) for the inhibitors.

This screening methodology can be easily tailored to accommodate testing of different alloys and various electrolyte solutions. This is especially convenient for future work that seeks to model alkaline conditions, a common environment encountered in steel-reinforced concrete applications. Further adjustments to the testing duration in the initial LPR screening may also be easily implemented to better suit certain applications. Additionally, qualifications of an effective inhibitor in this work were benchmarked as those that achieved sustained inhibition efficiencies of greater than 50%, however this selection criterion could be adjusted to allow more or less inhibitors through the screening process. This may be necessary in situations based on factors such as a cost-benefit analysis or where tradeoffs in efficiency are permitted for similar reasons. In these instances, the proposed methodology still provides a framework for screening inhibitors, but is adaptable to fit specific research needs if necessary.

4.3. Future Work

The research presented in this work is intended to provide the groundwork for future organic corrosion inhibitor studies, as well as test method development involving electrochemical and interfacial characterization of these chemicals on metal substrates. There were multiple

tangents throughout the process of this work that were not explored, however they still warrant further investigation and are presented here as potential avenues for future research, especially in regard to formulating a more comprehensive characterization method while still maintaining the same pace in data acquisition and ease of interpreting results.

Further studies exploring the use of electrochemical impedance spectroscopy (EIS), especially in determining an inhibitor application procedure that allows for useful discrimination of results, would provide an electrochemical method capable of correlating inhibitor function to the formation of an adsorbed layer, as well as corrosion rate calculation from polarization resistance (R_p) determination. Of particular interest is the effect of inhibitor concentration and the extent of surface coverage calculated via change of the modeled double layer capacitance (C_{dl}) circuit element.

The research possibilities offered by the QCM are numerous, and further exploration with this instrument is recommended. A repeat of the experiments in this work with an Fe-coated quartz crystal is recommended in order to examine more realistic adsorption behavior to a mild steel surface. Additionally, studying the inhibitor sans electrolyte has the potential of offering a more ideal adsorption mechanism as there is no competitive adsorption between the inhibitor molecules and the electrolyte. In this work, a preliminary investigation utilizing OCP monitoring was performed in conjunction with several QCM experiments in order to examine the change in corrosion potential as the inhibitor adsorbed to the substrate surface. Initial results show a strong correlation between adsorption on the electrode surface and change in corrosion potential; it would be beneficial to investigate this further, as well as the use of other electrochemical experiments in conjunction with QCM testing.

Exchanging the QCM static cell used in this work for a flow cell, where solution is continuously pumped over the quartz crystal surface, opens up more research opportunities while reducing noise in the data due to clumsy additions of concentrated inhibitor solutions mid-experiment. The flow cell is capable of continuous data collection under changing solution characteristics, enabling the study of real time changes in inhibitor concentration. Such an experiment would result in a continuous *concentration vs. mass change* curve, making adsorption isotherm calculations relatively easy. Additionally, future studies with a QCM flow cell examining the desorption process by flushing the cell after initial adsorption may prove interesting and shed light on adsorption strength of the inhibitor molecule. Furthermore, the effects of changing pH or dissolved oxygen content are of particular interest.

Future work might focus on alterations to the surface characterization method to alleviate atmospheric contamination of the samples, either by shortening the period between inhibitor application and XPS testing, or by adding a cleaning step that leaves the adsorbed molecules undisturbed. Additional surface characterization may involve incorporation of scanning electron microscopy to obtain surface images of effective and ineffective inhibitor systems for comparison. Further studies might also examine the use of energy-dispersive X-ray spectroscopy (EDS) in comparison (or even replacement) to XPS, with a focus on data quality and cost per experiment. Furthermore, inductively coupled plasma atomic emission spectroscopy (ICP-AES) might be performed to determine the elemental composition of the electrolyte after corrosion has taken place; an imbalance of a particular element in solution when compared to the alloy composition suggests that this element receives less protection from the adsorbed inhibitor and is preferentially leached from the metal. Such an experiment may help determine favorable sites for adsorption by organic inhibitors.